PHYSICAL REVIEW D **79,** 043008 (2009)

Thermalization of the mildly relativistic plasma

A. G. Aksenov

Institute for Theoretical and Experimental Physics, B. Cheremushkinskaya 25, 117218 Moscow, Russia
and Institute for Computer-Aided Design, Russian Academy of Sciences, Vtoraya Brestskaya 19/18, Moscow, 123056, Russia

R. Ruffini and G. V. Vereshchagin

ICRANet p.le della Repubblica, 10, 65100 Pescara, Italy
and ICRA and University of Rome "Sapienza", Physics Department, p.le A. Moro 5, 00185 Rome, Italy

(Received 12 September 2008; published 18 February 2009)

In a recent paper [A. G. Aksenov, R. Ruffini, and G. V. Vereshchagin, Phys. Rev. Lett. **99**, 125003 (2007).] we considered the approach of nonequilibrium pair plasma towards a thermal equilibrium state adopting a kinetic treatment and solving numerically the relativistic Boltzmann equations. It was shown that plasma in the energy range 0.1–10 MeV reaches kinetic equilibrium first, on a time scale $t_{\rm k} \lesssim 10^{-14}$ sec, with detailed balance between binary interactions such as Compton, Bhabha, and Møller scattering, and pair production and annihilation. Later the electron-positron-photon plasma approaches thermal equilibrium on a time scale $t_{\rm th} \lesssim 10^{-12}$ sec, with detailed balance for all direct and inverse reactions. In the present paper we systematically present details of the computational scheme used there, as well as generalize our treatment, considering proton loading of the pair plasma. When proton loading is large, protons thermalize first by proton-proton scattering, and then, with the electron-positron-photon plasma, by proton-electron scattering. In the opposite case of small proton loading, proton-electron scattering dominates over proton-proton scattering. Thus in all cases the plasma, even with a proton admixture, reaches a thermal equilibrium configuration on a time scale $t_{\rm th} \lesssim 10^{-11}$ sec. We show that it is crucial to account for not only binary but also triple direct and inverse interactions between electrons, positrons, photons, and protons. Several explicit examples are given, and the corresponding time scales for reaching kinetic and thermal equilibria are determined.

DOI: 10.1103/PhysRevD.79.043008 PACS numbers: 52.27.Ep, 05.20.Dd

I. INTRODUCTION

Electron-positron plasma is of interest in many fields of physics and astrophysics. In the early Universe [1–4] during the lepton era, ultrarelativistic electron-positron pairs contributed to the matter content of the Universe. In gamma-ray bursts (GRBs) electron-positron pairs play an essential role in the dynamics of expansion [5–7]. Indications exist that the pair plasma is present also in active galactic nuclei [8], in the center of our Galaxy [9], around hypothetical quark stars [10]. In the laboratory pair plasma is expected to appear in the fields of ultra intense lasers [11], where particle production may serve as a diagnostic tool for high-energy plasma [12].

In many stationary astrophysical sources the pair plasma is thought to be in thermodynamic equilibrium. A detailed study of the relevant processes [13–18], radiation mechanisms [19], possible equilibrium configurations [15,20,21], and spectra [22] in an optically thin pair plasma has been carried out. Particular attention has been given to collisional relaxation processes [23,24], pair production and annihilation [25], relativistic bremsstrahlung [26,27], and double Compton scattering [28,29].

An equilibrium occurs if the sum of all reaction rates vanishes. For instance, electron-positron pairs are in equilibrium when the net pair production (annihilation) rate is zero. This can be achieved in a variety of ways, and the corresponding condition can be represented as a system of algebraic equations [30]. However, the main assumption made in all the above-mentioned works is that electrons, positrons, and protons (photons) obey, respectively, Fermi-Dirac (Bose-Einstein) distributions. The latter is shown to be possible, in principle, in the range of temperatures up to 10 MeV [13,24]. Our main task is to prove that, independently of a wide set of initial conditions, thermal equilibrium forms when the phase space distribution functions are recovered during the process of thermalization by two-body and three-body direct and inverse particle-particle collisions.

At the same time, in some of the cases mentioned above the pair plasma can be optically thick. Although moderately thick plasmas have been considered in the literature [21], a qualitative description [13,20] is only available for large optical depths. An assumption of thermal equilibrium is often adopted for rapidly evolving systems such as GRBs without explicit proof [5–7,31]. Then, a hydrodynamic approximation is usually applied for both leptons and photons. However, particles may not be in equilibrium initially. Moreover, they may not reach equilibrium in rapidly evolving systems such as the early Universe or transient events, when the energy is released on a very short time scale.

In the literature there is no consensus on this point. Some authors considered thermal equilibrium as the initial state

prior to expansion [5,7], while others did not [32]. In fact, the detailed study of the pair plasma equilibrium configurations, performed in [20], cannot answer this question, because essentially nonequilibrium processes have to be considered.

Thus, observations provide motivation for theoretical analysis of physical conditions taking place in nonequilibrium optically thick pair plasma. Notice that there is a substantial difference between ion-electron plasma and electron-positron plasma. First, the former is collisionless in a wide range of parameters [33], while collisions are always essential in the latter. Second, when collisions are important, the relevant interactions in the former case include Coulomb scattering of particles, which is usually described by the classical Rutherford cross section. In contrast, interactions in the pair plasma are described by quantum cross sections even if the plasma itself can still be treated as a classical one.

In [34,35] we clarified the issue of the initial state of the pair plasma in GRBs sources in the case of pure pair plasma. Our numerical calculations show that the pair plasma on a time scale $t \lesssim 10^{-12}$ sec reaches thermal equilibrium prior to expansion, due to intense binary and triple collisions. In this paper we present details about the computational scheme adopted in [34] and turn to a more general case, the pair plasma loaded with baryons. The occurrence of the thermalization process and the corresponding time scales is necessary for determining the dynamics of GRBs. Thermalization time scales $t \lesssim 10^{-12}$ sec are indeed necessary in order to relate the observed properties of GRBs to the nature of the source; see e.g. [36].

In the next section we give a qualitative description of the pair plasma, introducing some relevant parameters. In Sec. III we discuss pure pair plasma. In Sec. IV pair plasma with proton loading is discussed. In Sec. V we describe the computational scheme used in our analysis. In Sec. VI we present results of our numerical computations. A discussion and conclusions follow in the last section. In Appendix A relevant conservation laws are recalled. In Appendix B conditions for kinetic and thermal equilibria are formulated, and the scheme for the determination of temperatures and chemical potentials out of number and energy densities is given. Binary interactions in the pair plasma such as Compton, Møller, and Bhabha scatterings, as well as pair creation and annihilation by two photons are discussed in Appendix C. In Appendix D Compton and Coulomb scatterings with protons are considered. In Appendix E three-body radiative variants of the reactions listed above are given. Cutoff schemes for the numerical evaluation of emission and absorption coefficients are presented in Appendix F. In Appendix G mass scaling of the matrix elements for Coulomb scattering between electrons, positrons, and protons is discussed. In Appendix H the definitions of matrix elements and cross sections adopted in the paper are given.

II. QUALITATIVE DESCRIPTION OF THE PAIR PLASMA

First of all, we specify the domain of parameters characterizing the pair plasma considered in this paper. It is convenient to use dimensionless parameters usually adopted for this purpose.

We consider mildly relativistic pair plasma; thus the average energy per particle ϵ brackets the electron rest mass energy,

$$0.1 \lesssim \frac{\epsilon}{mc^2} \lesssim 10. \tag{1}$$

The lower boundary is required for significant concentration of pairs, while the upper boundary is set to avoid substantial production of other particles such as muons and neutrinos.

We define the plasma parameter $\mathfrak{g} = (n_- d^3)^{-1}$, where $d = \sqrt{\frac{k_B T_-}{4\pi e^2 n_-}} = \frac{c}{\omega}\sqrt{\theta_-}$ is the Debye length; k_B is Boltzmann's constant; e, n_-, and T_- are the electron charge, number density and temperature, respectively; c is the speed of light; $\theta_- = k_B T_-/(mc^2)$ is the dimensionless temperature; $\omega = \sqrt{4\pi e^2 n_-/m}$ is the plasma frequency; and m is the electron mass. To ensure the applicability of the kinetic approach, the plasma parameter must be small, $\mathfrak{g} \ll 1$. This condition means that the kinetic energy of particles dominates their potential energy due to mutual interaction. For the pair plasma considered in this paper, this condition is satisfied.

Further, the classicality parameter, defined as $\varkappa = e^2/(\hbar v_r) = \alpha/\beta_r$, where $\hbar$ is Planck's constant, $\alpha = e^2/(\hbar c)$ is the fine structure constant and $v_r = \beta_r c$ is the mean relative velocity of particles; see (F12). The condition $\varkappa \gg 1$ means that particle collisions can be considered classically, while for $\varkappa \ll 1$ a quantum description is required. In our case, for both pairs and protons quantum cross sections are used since $\varkappa < 1$.

The strength of screening of the Coulomb interactions is characterized by the Coulomb logarithm $\Lambda = \mathcal{M} d v_r/\hbar$, where $\mathcal{M}$ is the reduced mass. For electron-electron or electron-positron scattering the reduced mass is just $m/2$, while for electron-proton or positron-proton scattering the reduced mass is just the proton mass $\mathcal{M} \simeq M$; for proton-proton scattering $\mathcal{M} \simeq M/2$. The Coulomb logarithm varies with the mean particle velocity and Debye length, and it cannot be set as a constant as is usually done in most studies of the pair plasma.

Finally, we consider pair plasma with linear dimensions R exceeding the mean free path of photons $l = (n_- \sigma)^{-1}$, where σ is the corresponding total cross section. Thus the optical depth $\tau = n\sigma R \gg 1$ is large, and interactions between photons and other particles have to be taken into account. We discuss these interaction in the next section.

Note that natural parameters for perturbative expansion in the problem under consideration are the fine-structure constant α and the electron-proton mass ratio m/M.

III. PURE PAIR PLASMA

For simplicity, we first consider pure pair plasma composed of electrons e^-, positrons e^+, and photons γ. We will turn to a more general case, including protons p, in the next section. We assume that pairs or photons appear from some physical process in the region with size R and on a time scale $t < R/c$. We further assume that distribution functions of particles depend neither on spatial coordinates nor on the direction of momenta. We then have $f_i = f_i(\epsilon, t)$; namely, we consider isotropic distribution functions in momentum space for a spatially uniform and isotropic plasma.

To make sure that the classical kinetic description is adequate, we estimate the dimensionless degeneracy temperature

$$\theta_F = \left[\left(\frac{\hbar}{mc}\right)^2 (3\pi^2 n_-)^{2/3} + 1\right]^{1/2} - 1, \tag{2}$$

and compare it with the estimated temperature in thermal equilibrium. With our initial conditions (1) the degeneracy temperature is always smaller than the temperature in thermal equilibrium, and therefore we can safely apply the classical kinetic approach. Besides, since we deal with an ideal plasma with the plasma parameter $\mathfrak{g} \sim 10^{-3}$, it is enough to consider only one-particle distribution functions. These conditions justify our computational approach based on the classical relativistic Boltzmann equation. At the same time, the right-hand side of the Boltzmann equation contains collisional integrals as functions of quantum matrix elements, as discussed below and in Appendixes C, D, and E.

Relativistic Boltzmann equations [37,38] in the spherically symmetric case for which the original code is designed [39] are

$$\frac{1}{c}\frac{\partial f_i}{\partial t} + \beta_i\left(\mu\frac{\partial f_i}{\partial r} + \frac{1-\mu^2}{r}\frac{\partial f_i}{\partial \mu}\right) - \nabla U\frac{\partial f_i}{\partial \mathbf{p}} = \sum_q (\eta_i^q - \chi_i^q f_i), \tag{3}$$

where $\mu = \cos\vartheta$, ϑ is the angle between the radius vector $\mathbf{r}$ from the origin and the particle momentum $\mathbf{p}$, U is a potential due to an external force, $\beta_i = v_i/c$ are particles velocities, $f_i(\epsilon, t)$ are their distribution functions, the index i denotes the type of particle, ϵ is its energy, and η_i^q and χ_i^q are the emission and the absorption coefficients for the production of a particle of type "i" via the physical process labeled by q. This is a coupled system of partial-integrodifferential equations. For homogeneous and isotropic distribution functions of electrons, positrons, and photons, (3) reduces to

$$\frac{1}{c}\frac{\partial f_i}{\partial t} = \sum_q (\eta_i^q - \chi_i^q f_i), \tag{4}$$

which is a coupled system of integrodifferential equations. In (4) we also explicitly neglected the Vlasov term, describing the collisionless interaction of particles in the mean field, since the energy density of fluctuations of the electromagnetic field is many orders of magnitude smaller than the energy density of particles [40].

Therefore, the left-hand side of the Boltzmann equation is reduced to the partial derivative of the distribution function with respect to time. The right-hand side contains collisional integrals, representing interactions between electrons, positrons, and photons.

As an example of a collisional integral, we consider the absorption coefficient for Compton scattering which is given by

$$\chi^{\rm cs} f_\gamma = \int d\mathbf{k}' d\mathbf{p} d\mathbf{p}' W_{\mathbf{k}',\mathbf{p}';\mathbf{k},\mathbf{p}} f_\gamma(\mathbf{k}, t) f_\pm(\mathbf{p}, t), \tag{5}$$

where $\mathbf{p}$ and $\mathbf{k}$ are momenta of the electron (positron) and the photon, respectively, $d\mathbf{p} = d\epsilon_\pm do \epsilon_\pm^2 \beta_\pm/c^3$, $d\mathbf{k}' = d\epsilon_\gamma' \epsilon_\gamma'^2 do_\gamma'/c^3$, and the transition function $W_{\mathbf{k}',\mathbf{p}';\mathbf{k},\mathbf{p}}$ is related to the transition probability differential $dw_{\mathbf{k}',\mathbf{p}';\mathbf{k},\mathbf{p}}$ per unit time as

$$W_{\mathbf{k}',\mathbf{p}';\mathbf{k},\mathbf{p}} d\mathbf{k}' d\mathbf{p}' \equiv V dw_{\mathbf{k}',\mathbf{p}';\mathbf{k},\mathbf{p}}. \tag{6}$$

The differential probability $dw_{\mathbf{k}',\mathbf{p}';\mathbf{k},\mathbf{p}} = w_{\mathbf{k}',\mathbf{p}';\mathbf{k},\mathbf{p}} d\mathbf{k}' d\mathbf{p}'$ is given by (C3) in Appendix C.

Given the momentum conservation, one can perform one integration over $d\mathbf{p}'$ in (5) as

$$\int d\mathbf{p}' \delta(\mathbf{k} + \mathbf{p} - \mathbf{k}' - \mathbf{p}') \to 1, \tag{7}$$

but it is necessary to take into account the momentum conservation in the next integration over $d\mathbf{k}'$, so we have

$$\begin{aligned}\int d\epsilon_\gamma' \delta(\epsilon_\gamma + \epsilon_\pm - \epsilon_\gamma' - \epsilon_\pm') &= \int d(\epsilon_\gamma' + \epsilon_\pm') \frac{1}{|\partial(\epsilon_\gamma' + \epsilon_\pm')/\partial\epsilon_\gamma'|} \\ &\times \delta(\epsilon_\gamma + \epsilon_\pm - \epsilon_\gamma' - \epsilon_\pm') \\ &\to \frac{1}{|\partial(\epsilon_\gamma' + \epsilon_\pm')/\partial\epsilon_\gamma'|} \equiv J_{\rm cs},\end{aligned} \tag{8}$$

where the Jacobian of the transformation is

$$J_{\rm cs} = \frac{1}{1 - \beta_\pm' \mathbf{b}_\gamma' \cdot \mathbf{b}_\pm'}, \tag{9}$$

and $\mathbf{b}_i = \mathbf{p}_i/p$, $\mathbf{b}_i' = \mathbf{p}_i'/p'$, $\mathbf{b}_\pm' = (\beta_\pm \epsilon_\pm \mathbf{b}_\pm + \epsilon_\gamma \mathbf{b}_\gamma - \epsilon_\gamma' \mathbf{b}_\gamma')/(\beta_\pm' \epsilon_\pm')$.

Finally, for the absorption coefficient we have

$$\chi^{\rm cs} f_\gamma = -\int do'_\gamma d\mathbf{p} \frac{\epsilon'_\gamma |M_{fi}|^2 \hbar^2 c^2}{16 \epsilon_\pm \epsilon_\gamma \epsilon'_\pm} J_{\rm cs} f_\gamma(\mathbf{k}, t) f_\pm(\mathbf{p}, t), \tag{10}$$

where the matrix element here is dimensionless. This integral is evaluated numerically, as described in Appendix C.

For all binary interactions we use exact QED matrix elements which can be found in the standard textbooks, e.g. in [41–43], and are given in Appendix C.

In order to account for the charge screening, we introduced the minimal scattering angles following [44]; see Appendix F. This allows us to apply the same scheme for the computation of emission and absorption coefficients for Coulomb scattering, while many treatments in the literature use the Fokker-Planck approximation; see e.g. [45].

For such a dense plasma, collisional integrals in (2) should include not only binary interactions, having order α^2 in Feynmann diagrams, but also triple ones, having order α^3 [41]. As an example of triple interactions, consider relativistic bremsstrahlung,

$$e_1 + e_2 \leftrightarrow e'_1 + e'_2 + \gamma'. \tag{11}$$

For the time derivative, for instance, of the distribution function f_2 in the direct and inverse reactions (11), one has

$$\begin{aligned} \dot{f}_2 &= \int d\mathbf{p}_1 d\mathbf{p}'_1 d\mathbf{p}'_2 d\mathbf{k}' [W_{\mathbf{p}'_1,\mathbf{p}'_2,\mathbf{k}';\mathbf{p}_1,\mathbf{p}_2} f'_1 f'_2 f'_k \\ &\quad - W_{\mathbf{p}_1,\mathbf{p}_2;\mathbf{p}'_1,\mathbf{p}'_2,\mathbf{k}'} f_1 f_2] \\ &= \int d\mathbf{p}_1 d\mathbf{p}'_1 d\mathbf{p}'_2 d\mathbf{k}' \frac{c^6 \hbar^3}{(2\pi)^2} \frac{\delta^{(4)}(P_f - P_i) |M_{fi}|^2}{2^5 \epsilon_1 \epsilon_2 \epsilon'_1 \epsilon'_2 \epsilon'_\gamma} \\ &\quad \times \left[f'_1 f'_2 f'_k - \frac{1}{(2\pi\hbar)^3} f_1 f_2 \right], \end{aligned} \tag{12}$$

where

$$\begin{aligned} d\mathbf{p}_1 d\mathbf{p}_2 W_{\mathbf{p}'_1,\mathbf{p}'_2,\mathbf{k}';\mathbf{p}_1,\mathbf{p}_2} &\equiv V^2 dw_1, \\ d\mathbf{p}'_1 d\mathbf{p}'_2 d\mathbf{k}' W_{\mathbf{p}_1,\mathbf{p}_2;\mathbf{p}'_1,\mathbf{p}'_2,\mathbf{k}'} &\equiv V dw_2, \end{aligned}$$

and dw_1 and dw_2 are given by (H3) for the inverse and direct processes (11), respectively. The matrix element here has dimensions of length squared; see Appendix H.

In the case of the distribution functions (15), see below, we have multipliers proportional to

$$F_i = \exp \frac{\nu_i}{\theta_i}, \tag{13}$$

called fugacities, in front of the integrals. The calculation of emission and absorption coefficients is then reduced to the well-known thermal equilibrium case [30]. In fact, since reaction rates of triple interactions are α times smaller than binary reaction rates, we expect that binary reactions come into detailed balance first. Only when binary reactions are all balanced, do triple interactions become important. In addition, when binary reactions come into balance, distribution functions already acquire the form (15). Although there is no principal difficulty in computations using exact matrix elements for triple reactions as well, our simplified scheme allows for much faster numerical computation. The corresponding reaction rates for triple interactions are given in Appendix E.

We consider all possible binary and triple interactions between electrons, positrons, and photons, as summarized in Table I.

Each of the above-mentioned reactions is characterized by the corresponding time scale and optical depth. For Compton scattering of an electron, for instance, we have

$$t_{\rm cs} = \frac{1}{\sigma_T n_\pm c}, \qquad \tau_{\rm cs} = \sigma_T n_\pm R, \tag{14}$$

where $\sigma_T = \frac{8\pi}{3} \alpha^2 (\frac{\hbar}{mc})^2$ is the Thomson cross section. There are two time scales in our problem that characterize the condition of detailed balance between direct and inverse reactions, $t_{\rm cs}$ for binary interactions and $\alpha^{-1} t_{\rm cs}$ for triple interactions, respectively.

We choose arbitrary initial distribution functions and find a common development. At a certain time $t_{\rm k}$ the distribution functions always evolve in a functional form over the entire energy range, and depend only on two parameters. We find, in fact, for the distribution functions the expressions

$$f_i(\varepsilon) = \frac{2}{(2\pi\hbar)^3} \exp\left(-\frac{\varepsilon - \nu_i}{\theta_i} \right), \tag{15}$$

with chemical potential $\nu_i \equiv \frac{\varphi_i}{mc^2}$ and temperature $\theta_i \equiv \frac{k_B T_i}{m_e c^2}$, where $\varepsilon \equiv \frac{\epsilon}{m_e c^2}$ is the energy of the particle. Such a configuration corresponds to a kinetic equilibrium [2,45,46] in which particles acquire a common temperature and nonzero chemical potentials. At the same time, we found that triple interactions become essential for $t > t_{\rm k}$, after the establishment of kinetic equilibrium. In a strict mathematical sense, the sufficient condition for reaching thermal equilibrium is when each direct reaction is exactly balanced with its inverse. Therefore, in principle, not only triple interactions, but also four-particle interactions, five-particle interactions, etc. have to be accounted for in Eq. (4). The time scale for reaching thermal equilibrium will then be determined by the slowest reaction which is not balanced with its inverse. We stress, however, that the necessary condition is the detailed balance, at least in triple interactions, since binary reactions do not change chemical potentials.

Notice that a method similar to ours was applied in [45] in order to compute spectra of particles in kinetic equilibrium. However, although the approach was similar, the computation was never carried out in order to actually observe thermal equilibrium being reached.

TABLE I. Microphysical processes in the pair plasma.

Binary interactions	Radiative and pair producing variants
Møller and Bhabha	Bremsstrahlung
$e_1^{\pm} e_2^{\pm} \rightarrow e_1^{\pm\prime} e_2^{\pm\prime}$	$e_1^{\pm} e_2^{\pm} \leftrightarrow e_1^{\pm\prime} e_2^{\pm\prime} \gamma$
$e^{\pm} e^{\mp} \rightarrow e^{\pm\prime} e^{\mp\prime}$	$e^{\pm} e^{\mp} \leftrightarrow e^{\pm\prime} e^{\mp\prime} \gamma$
Single Compton	Double Compton
$e^{\pm} \gamma \rightarrow e^{\pm} \gamma'$	$e^{\pm} \gamma \leftrightarrow e^{\pm\prime} \gamma' \gamma''$
Pair production and annihilation	Radiative pair production and three-photon annihilation
$\gamma \gamma' \leftrightarrow e^{\pm} e^{\mp}$	$\gamma \gamma' \leftrightarrow e^{\pm} e^{\mp} \gamma''$
	$e^{\pm} e^{\mp} \leftrightarrow \gamma \gamma' \gamma''$
	$e^{\pm} \gamma \leftrightarrow e^{\pm\prime} e^{\mp} e^{\pm\prime\prime}$

Finally, it is worth mentioning the physical meaning of the chemical potential ν_{k} in kinetic equilibrium entering the formula (15). In the case of pure pair plasma a nonzero chemical potential represents deviation from thermal equilibrium through the relation

$$\nu_{\mathrm{k}} = \theta \ln(n_{\mathrm{k}}/n_{\mathrm{th}}), \tag{16}$$

where n_{th} are concentrations of particles in thermal equilibrium.

IV. PROTON LOADING

So far, we dealt with leptons having the same mass but opposite charges. In that case the condition of electric neutrality is identically fulfilled. We described electrons and positrons with the same distribution function. The situation becomes more complicated when an admixture of protons is allowed. Since charge neutrality

$$n_- = n_+ + n_p \tag{17}$$

is required, the number of electrons is not equal to the number of protons. In such a case a new dimensionless parameter, the baryonic loading $\mathbf{B}$, can be introduced as

$$\mathbf{B} = \frac{NMc^2}{\mathcal{E}} = \frac{n_p Mc^2}{\rho_r}, \tag{18}$$

where N and n_p are the number and the concentration of protons, and $\mathcal{E}$ and $\rho_r = \rho_\gamma + \rho_+ + \rho_-$ are radiative energy and energy density, respectively. Since in relativistic plasma, electrons and positrons move at almost the speed of light, both photons and pairs in thermal equilibrium behave as a relativistic fluid with an equation of state $p_r \simeq \rho_r/3$. At the same time, protons are relatively cold particles in the energy range (1), with negligible pressure and a dustlike equation of state $p \simeq 0$. In this way, by introducing parameter $\mathbf{B}$, we distinguish a radiation-dominated plasma ($\mathbf{B} < 1$) from a matter-dominated ($\mathbf{B} > 1$) plasma. For electrically neutral plasmas there exists an upper limit on the parameter $\mathbf{B}$ defined by (18), which is $\mathbf{B} \leq M/m$.

In the range of energies (1) the radiative energy density can be approximated as $\rho_r \sim n_- mc^2$, and then we have $n_p \sim n_- \mathbf{B} \frac{m}{M}$ for concentrations. If protons and electrons are at the same temperature, then from the equality of the kinetic energy of a proton $\epsilon_{k,p} = \frac{Mv_p^2}{2}$ and the one of an electron $\epsilon_{k,-} \sim mc^2$, we have $\frac{v_p}{c} \sim \sqrt{\frac{m}{M}}$; therefore protons are indeed nonrelativistic.

In the presence of protons additional binary reactions consist of Coulomb collisions between electrons (positrons) and protons, scattering of protons on protons, and Compton scattering of protons. Additional triple reactions are radiative variants of these reactions; see Table II and Appendix D.

Protons can be thermalized first by proton-proton collisions and then by electron/positron-proton collisions, or alternatively just by the latter mechanism, depending on the corresponding time scales. The rate of proton-proton collisions is a factor $\sqrt{\frac{m}{M}} \frac{n_p}{n_-} \sim \mathbf{B}(\frac{m}{M})^{3/2}$ smaller than the rate of electron-electron collisions; see (D15). The rate of proton-electron/positron collisions is a factor $\frac{\epsilon}{Mc^2} \sim \frac{m}{M}$ smaller than the one of electron-electron collisions; see (D11). Therefore, for $\mathbf{B} > \sqrt{\frac{m}{M}}$ proton-proton collisions are faster, while for $\mathbf{B} < \sqrt{\frac{m}{M}}$ proton-electron/positron ones predominate.

V. THE DISCRETIZATION PROCEDURE AND THE COMPUTATIONAL SCHEME

In order to solve Eqs. (4) we use a finite difference method by introducing a computational grid in the phase space to represent the distribution functions and to compute collisional integrals following [39]. Our goal is to

TABLE II. Microphysical processes in the pair plasma involving protons.

Binary interactions	Radiative and pair producing variants
Coulomb scattering	Bremsstrahlung
$p_1 p_2 \rightarrow p_1' p_2'$	$p_1 p_2 \leftrightarrow p_1' p_2' \gamma$
$p e^{\pm} \rightarrow p' e^{\pm\prime}$	$p e^{\pm} \leftrightarrow p' e^{\pm\prime} \gamma$
	$p e_1^{\pm} \leftrightarrow p' e_1^{\pm\prime} e^{\pm} e^{\mp}$
Single Compton	Double Compton
$p \gamma \rightarrow p' \gamma'$	$p \gamma \leftrightarrow p' \gamma' \gamma''$
	$p \gamma \leftrightarrow p' e^{\pm} e^{\mp}$

construct a scheme implementing energy, baryon number, and electric charge conservation laws; see Appendix A. For this reason we prefer to use in the code, instead of distribution functions f_i, the spectral energy densities

$$E_i(\epsilon_i) = \frac{4\pi\epsilon_i^3\beta_i f_i}{c^3}, \tag{19}$$

where $\beta_i = \sqrt{1-(m_i c^2/\epsilon_i)^2}$, in the phase space ϵ_i. Then

$$\epsilon_i f_i(\mathbf{p},t)d\mathbf{r}d\mathbf{p} = \frac{4\pi\epsilon^3\beta_i f_i}{c^3}d\mathbf{r}d\epsilon_i = E_i d\mathbf{r}d\epsilon_i \tag{20}$$

is the energy in the volume of the phase space $d\mathbf{r}d\mathbf{p}$. The number density of particles of type "i" is given by

$$n_i = \int f_i d\mathbf{p} = \int \frac{E_i}{\epsilon_i}d\epsilon_i, \qquad dn_i = f_i d\mathbf{p}, \tag{21}$$

while the corresponding energy density is

$$\rho_i = \int \epsilon_i f_i d\mathbf{p} = \int E_i d\epsilon_i.$$

We can rewrite the Boltzmann equations (4) in the form

$$\frac{1}{c}\frac{\partial E_i}{\partial t} = \sum_q (\tilde{\eta}_i^q - \chi_i^q E_i), \tag{22}$$

where $\tilde{\eta}_i^q = (4\pi\epsilon_i^3\beta_i/c^3)\eta_i^q$.

We introduced the computational grid for phase space $\{\epsilon_i, \mu, \phi\}$, where $\mu = \cos\vartheta$, ϑ, and ϕ are angles between the radius vector $\mathbf{r}$ and the particle momentum $\mathbf{p}$. The zone boundaries are $\epsilon_{i,\omega\mp1/2}$, $\mu_{k\mp1/2}$, $\phi_{l\mp1/2}$ for $1 \le \omega \le \omega_{\max}$, $1 \le k \le k_{\max}$, $1 \le l \le l_{\max}$. The length of the ith interval is $\Delta\epsilon_{i,\omega} \equiv \epsilon_{i,\omega+1/2} - \epsilon_{i,\omega-1/2}$. On the finite grid the functions (19) become

$$E_{i,\omega} \equiv \frac{1}{\Delta\epsilon_{i,\omega}}\int_{\Delta\epsilon_{i,\omega}} d\epsilon E_i(\epsilon). \tag{23}$$

Now we can replace the collisional integrals in (22) by the corresponding sums.

After this procedure we get the set of ordinary differential equations (ODE's), instead of the system of partial differential equations for the quantities $E_{i,\omega}$ to be solved. There are several characteristic times for different processes in the problem, and therefore our system of differential equations is stiff. Under these conditions eigenvalues of the Jacobi matrix differ significantly, and the real parts of the eigenvalues are negative. We use Gear's method [47] to integrate ODE's numerically. This high-order implicit method was developed for the solution of stiff ODE's.

In our method the exact energy conservation law is satisfied. For binary interactions the particle number conservation law is satisfied, as we adopt interpolation of grid functions $E_{i,\omega}$ inside the energy intervals.

VI. NUMERICAL RESULTS

In what follows we consider in detail three specific cases. In the first two cases our grid consists of 60 energy intervals and 16×32 intervals for two angles ϑ and ϕ characterizing the direction of the particle momentum. In the third case we have 40 energy intervals.

A. Case I

We take the following initial conditions: flat initial spectral densities $E_i(\epsilon_i) = \text{const}$ and total energy density $\rho = 10^{24}$ erg/cm^3. Plasma is composed of photons with a small amount of electron-positron pairs; the ratio between energy densities in photons and in electron-positron pairs $\zeta = \rho_\pm/\rho_\gamma = 10^{-5}$. The baryonic loading parameter $\mathbf{B} = 10^{-3}$, corresponding to $\rho_p = 2.7 \times 10^{18}$ erg/cm^3.

The energy density in each component of plasma changes, as can be seen from Fig. 1, keeping constant the total energy density shown by the dotted line in Fig. 1, as the energy conservation requires. As early as at 10^{-23} sec the energy starts to be redistributed between electrons and positrons on the one hand, and between electrons and photons on the other hand, essentially by the pair-creation process. This leads to equipartition of energies between these particles at 3×10^{-15} sec. Concentrations of pairs and photons equalize at 10^{-14} sec, as can be seen from Fig. 2. From this moment, temperatures and chemical potentials of electrons, positrons, and photons tend to be equal (see Figs. 3 and 4, respectively), and this corresponds to the approach to kinetic equilibrium.

This is a quasiequilibrium state since the total number of particles is still approximately conserved, as can be seen

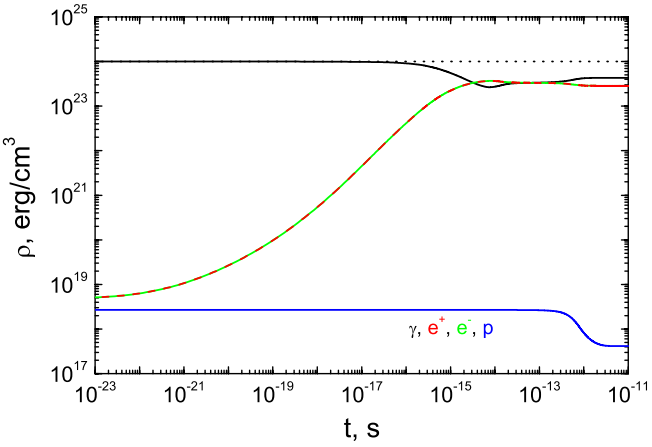

FIG. 1 (color online). Dependence on time of energy densities of electrons (green), positrons (red), photons (black), and protons (blue) for initial conditions I. The total energy density is shown by the dotted black line. Interaction between pairs and photons operates on very short time scales up to 10^{-23} sec. The quasiequilibrium state is established at $t_k \simeq 10^{-14}$ sec which corresponds to kinetic equilibrium for pairs and photons. Protons start to interact with them as late as at $t_{th} \simeq 10^{-13}$ sec.

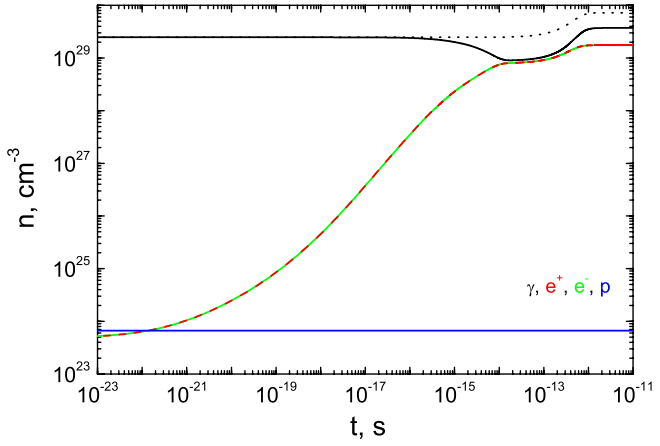

FIG. 2 (color online). Dependence on time of concentrations of electrons (green), positrons (red), photons (black), and protons (blue) for initial conditions I. The total number density is shown by the dotted black line. In this case kinetic equilibrium between electrons, positrons, and photons is reached at $t_k \simeq 10^{-14}$ sec. Protons join thermal equilibrium with other particles at $t_{th} \simeq 4 \times 10^{-12}$ sec.

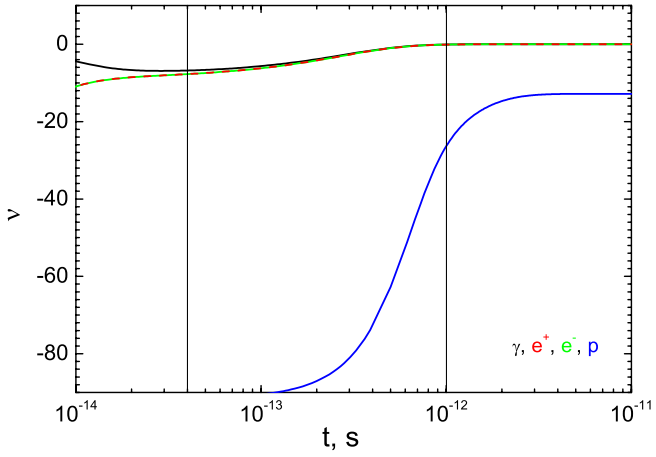

FIG. 4 (color online). Dependence on time of the dimensionless chemical potential of electrons (green), positrons (red), photons (black), and protons (blue) for initial conditions I. The chemical potential for pairs and photons acquires physical meaning only in kinetic equilibrium at $t_k \simeq 10^{-14}$ sec, while for protons this happens at $t_{th} \simeq 4 \times 10^{-12}$ sec. At this time the chemical potential of photons has evolved to zero and thermal equilibrium has already been reached.

from Fig. 2, and triple interactions are not yet efficient. At the moment $t_1 = 4 \times 10^{-14}$ sec, shown by the vertical line on the left in Figs. 3 and 4, the temperature of the photons and pairs is $\theta_k \simeq 1.5$, while the chemical potentials of these particles are $\nu_k \simeq -7$. The concentration of protons is so small that their energy density is not affected by the presence of other components; also, proton-proton collisions are inefficient. In other words, protons do not interact yet and their spectra are not yet of equilibrium form; see Fig. 5. The temperature of the protons starts to change only at 10^{-13} sec, when proton-electron Coulomb scattering becomes efficient.

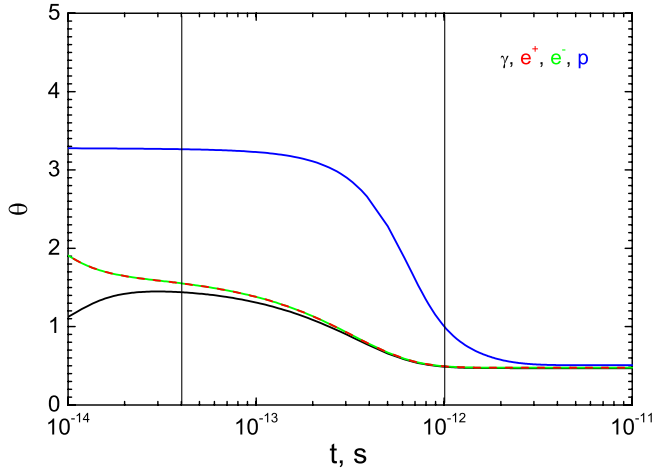

FIG. 3 (color online). Dependence on time of dimensionless temperatures of electrons (green), positrons (red), photons (black), and protons (blue) for initial conditions I. The temperature for pairs and photons acquires physical meaning only in kinetic equilibrium at $t_k \simeq 10^{-14}$ sec. Protons are cooled by the pair-photon plasma and acquire a common temperature with the plasma as late as at $t_{th} \simeq 4 \times 10^{-12}$ sec.

As can be seen from Fig. 4, the chemical potentials of electrons, positrons, and photons have evolved by that time due to triple interactions. Since the chemical potentials of electrons, positrons, and photons were negative, the particles were deficient with respect to the thermal state. This caused the total number of these particles to increase and, consequently, the temperature to decrease. The chemical potential of photons reaches zero at $t_2 = 10^{-12}$ sec, shown by the vertical line on the right in Figs. 3 and 4, which means that electrons, positrons, and photons are now in thermal equilibrium. However, protons are not yet in equilibrium with other particles since their spectra are not thermal, as shown in the lower part of Fig. 5.

Finally, the proton component thermalizes with other particles at 4×10^{-12} sec, and from that moment, plasma is characterized by a unique temperature, $\theta_{th} \simeq 0.48$, as Fig. 3 clearly shows. Protons have the final chemical potential $\nu_p \simeq -12.8$.

This state is characterized by the thermal distribution of all particles, as can be seen from Fig. 6. There, the initial flat density as well as the final spectral density are shown together with fits of particle spectra with the values of the common temperature and the corresponding chemical potentials in thermal equilibrium.

B. Case II

We take the following initial conditions: power-law spectral densities $E_i(\epsilon_i)$ for protons, electrons, and positrons with initial energy densities $\rho_p = 2.8 \times 10^{22}$ erg/cm^3,

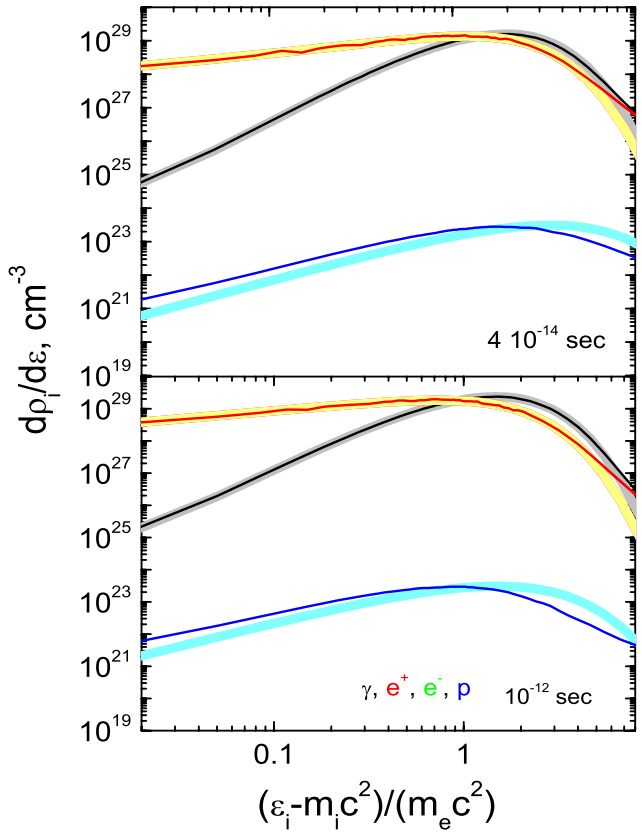

FIG. 5 (color online). Spectral density as a function of particle energy for electrons (green), positrons (red), photons (black), and protons (blue) for initial conditions I at intermediate time moments $t_1 = 4 \times 10^{-14}$ sec (upper figure) and $t_2 = 10^{-12}$ sec (lower figure). Fits of the spectra with chemical potentials and temperatures corresponding to the thermal equilibrium state are also shown by yellow (electrons and positrons), grey (photons), and light blue (protons) thick lines. The upper figure shows the spectra when kinetic equilibrium is established for the first time between electrons, positrons, and photons, while the lower figure shows the spectra at thermal equilibrium between these particles. In both figures protons are not yet in equilibrium, neither with themselves nor with other particles.

$\rho_- = 1.5 \times 10^{24}$ erg/cm^3, $\rho_+ = 1.5 \times 10^{21}$ erg/cm^3, respectively. We have chosen a flat spectral density for photons with $\rho_\gamma = 2.8 \times 10^{24}$ erg/cm^3. The initial baryonic loading parameter is set to $\mathbf{B} = 608$, corresponding to a matter-dominated plasma, unlike the previous case.

As in case I, the most rapid reaction is electron-positron pair creation, which starts to change the energy density of positrons at 10^{-20} sec ; see Fig. 7. Initially, most energy is in the photons, followed by electrons and protons. In the course of the evolution the energy gets redistributed in such a way that in the final state most of the energy is transferred first to the electrons, then to the protons and the photons, and finally to the positrons. In Fig. 8 one can see that number densities of electrons and protons are almost equal with the heavy proton loading chosen. Concentrations of

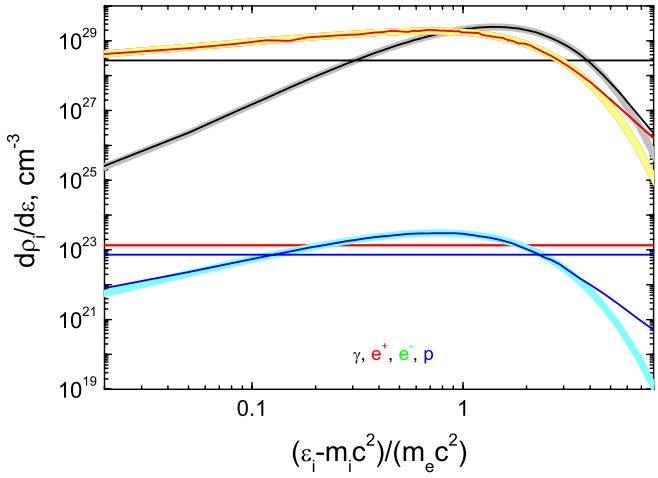

FIG. 6 (color online). The spectral density as a function of particle energy is shown as before at initial and final moments of the computations. The final photon spectrum is a blackbody one.

particles remain almost the same during the evolution towards thermal equilibrium.

Temperatures and chemical potentials of particles are shown in Figs. 9 and 10 respectively. Kinetic equilibrium is established at around 8×10^{-15} sec , marked by the vertical line. The temperature of pairs and photons at that moment is $\theta_k \simeq 0.53$, while the chemical potentials of these particles are $\nu_- \simeq 1$, $\nu_+ \simeq -0.9$, $\nu_\gamma \simeq 0.1$. Notice that chemical potentials of electrons and positrons are almost equal in magnitude and opposite in kinetic equilibrium; see Fig. 10. At this moment, protons are not yet in equilibrium with the rest of plasma but have already established kinetic equilibrium with themselves with the temperature $\theta_p \simeq 0.18$ and the chemical potential $\nu_p \simeq -2$. The common temperature is reached at the moment 10^{-13} sec , which corresponds to thermal equilibrium. The final value of the temperature is $\theta_{th} \simeq 0.47$, while chemical potentials are $\nu_\pm \simeq \mp 1$, $\nu_p \simeq -4.7$.

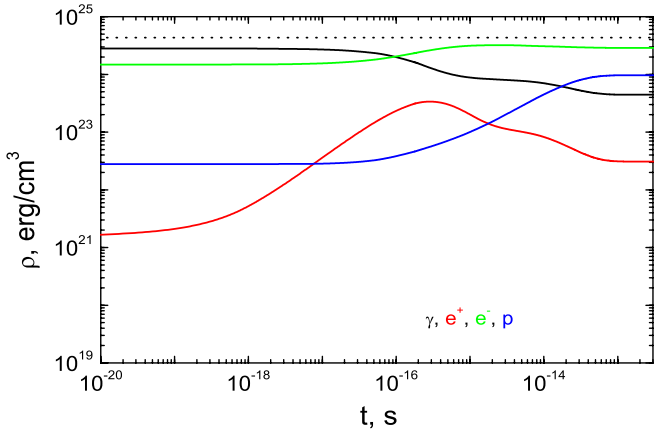

FIG. 7 (color online). Dependence on time of energy densities for initial conditions II. Colors are the same as in case I. Protons start to interact with other particles as late as at $t \simeq 10^{-16}$ sec .

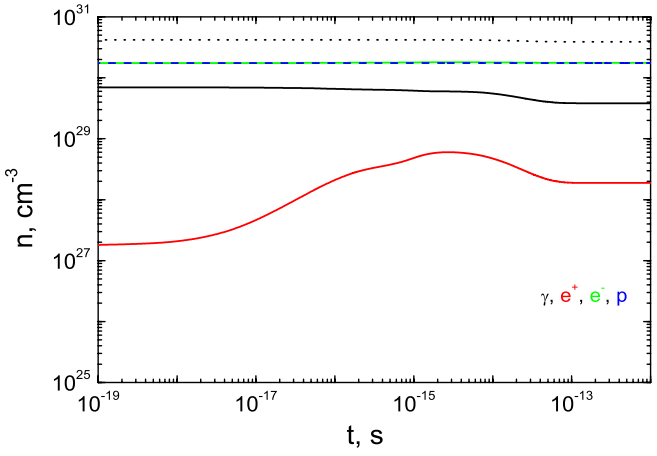

FIG. 8 (color online). Dependence on time of concentrations for initial conditions II. Colors are the same as in case I.

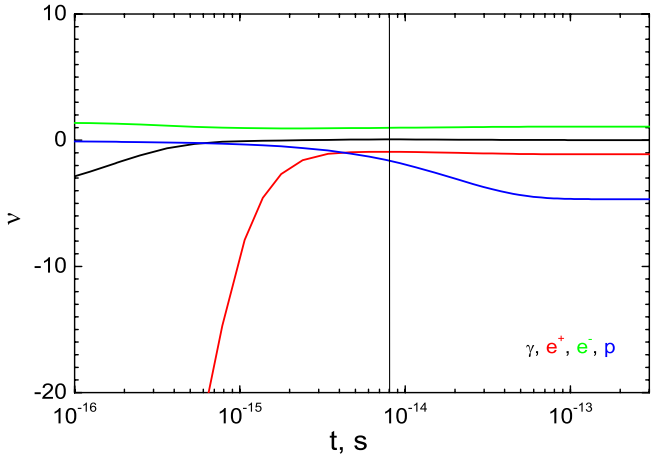

FIG. 10 (color online). Dependence on time of the dimensionless chemical potential for initial conditions II. Colors are the same as in case I. The chemical potential of the photons is almost zero in kinetic equilibrium. The chemical potentials of electrons and positrons are almost equal and opposite in kinetic equilibrium, to maintain electric neutrality.

The contribution of the protons to the total energy density increased over the course of time (see Fig. 7), causing an increase in the baryonic loading parameter, which reached the value $\mathbf{B} = 780$ in thermal equilibrium.

Since the concentration of protons is chosen to be large, proton-proton collisions become more important than proton-electron/positron collisions, in contrast to case I. In fact, the protons reach the equilibrium temperature already at 10^{-16} sec, while they start to interact with electrons and positrons only at 10^{-15} sec. Initial and final spectra of all particles are presented in Fig. 11.

C. Case III

We take the following initial conditions: the initial ratio between concentrations of electrons and protons is $\varsigma = n_p/n_- = 10^{-3}$. The total energy density is chosen in such a way that the final temperature in thermal equilibrium is $\theta_{\rm th} = 2$. We set up a flat initial spectrum for photons $E_\gamma(\epsilon_i) = \text{const}$, and power-law spectra for the pairs $E_\pm(\epsilon_\pm) \propto [\epsilon_\pm - mc^2]^{-2}$ and protons $E_p(\epsilon_p) \propto [\epsilon_p - Mc^2]^{-4}$. Finally, the ratio of initial and final concentrations of positrons is chosen to be $n_+ = 10^{-1} n_+^{\rm th}$. Given these initial conditions the baryon loading parameter is $\mathbf{B} = 0.2$.

The initial conditions are chosen in order to get larger temperatures in thermal equilibrium than in the previous cases. Unlike case II, the spectrum of protons is chosen to

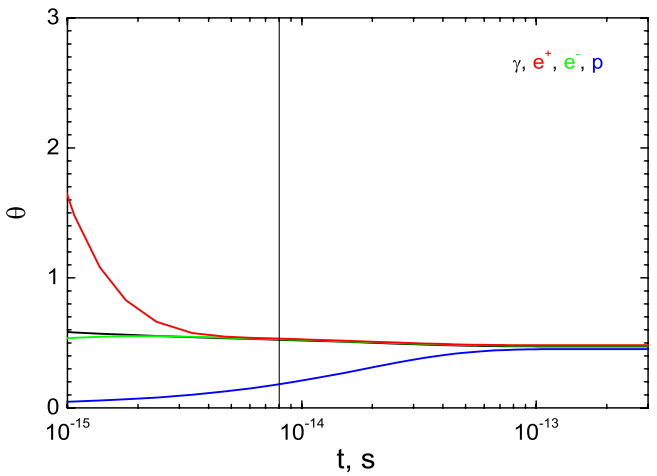

FIG. 9 (color online). Dependence on time of dimensionless temperature for initial conditions II. Colors are the same as in case I. The pair-photon plasma heats protons. Protons join thermal equilibrium at $t_{\rm th} \simeq 10^{-13}$ sec.

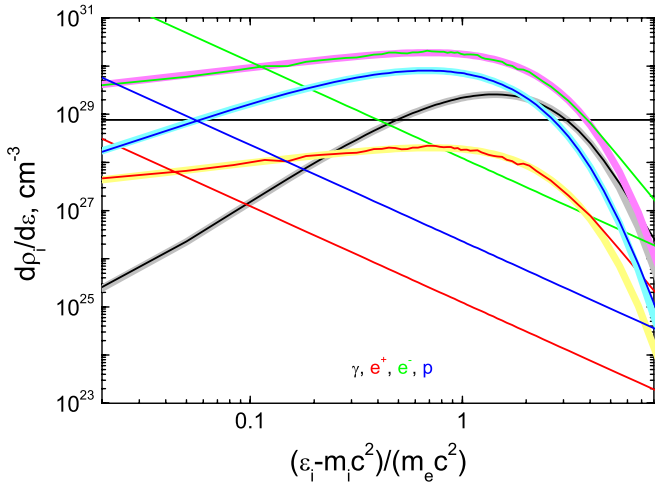

FIG. 11 (color online). Initial and final spectral densities as a function of particle energy for initial conditions II. Fits of the final spectra with chemical potentials and temperatures are also shown.

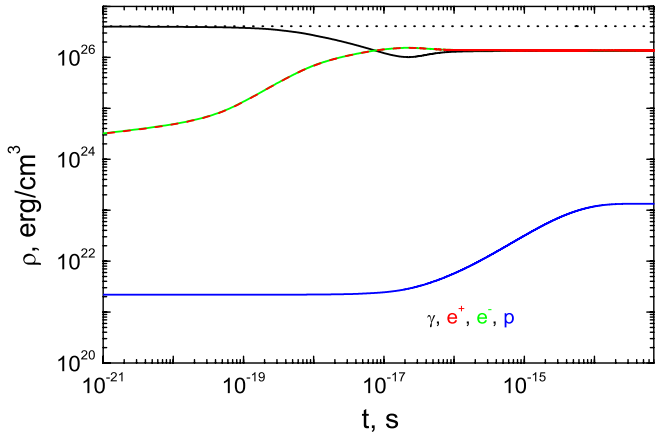

FIG. 12 (color online). Dependence on time of energy densities for initial conditions III. Colors are the same as in case I. Protons start to interact with other particles at about 10^{-17} sec.

be steeper than the spectrum of pairs in order to make them colder in kinetic equilibrium.

Equipartition of energies between pairs and photons occurs earlier than in case I, at around 10^{-17} sec (see Fig. 12), since now concentrations of particles are higher. Concentrations of pairs and photons equalize at 3×10^{-17} sec; see Fig. 13. As in case I, from this moment temperatures and chemical potentials of electrons, positrons, and photons tend to be equal (see Figs. 14 and 15, respectively), leading to kinetic equilibrium at around $t_k \simeq 10^{-16}$ sec.

At the moment t_k, shown by the vertical line on the left in Figs. 14 and 15, the temperature of photons and pairs is $\theta_k \simeq 2.2$, the chemical potential of these particles is $\nu_k \simeq -1.1$, while the temperature of protons, having a well-established spectrum by this time, is just $\theta_p \simeq 0.09$.

Thermal equilibrium is reached in the electron-positron-photon plasma at around $t_{th} \simeq 4 \times 10^{-15}$ sec, shown by

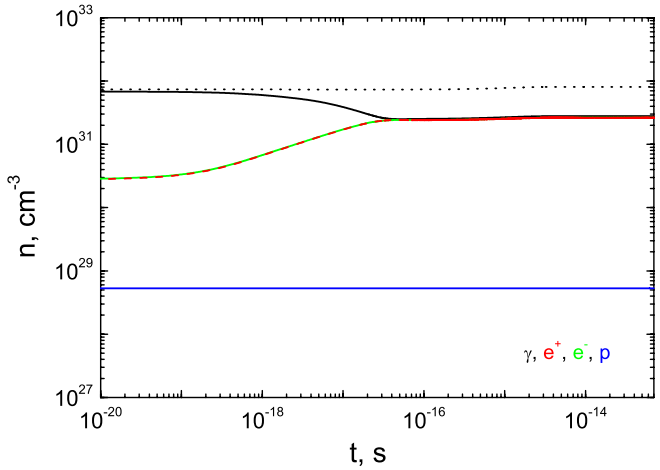

FIG. 13 (color online). Dependence on time of concentrations for initial conditions III. Colors are the same as in case I.

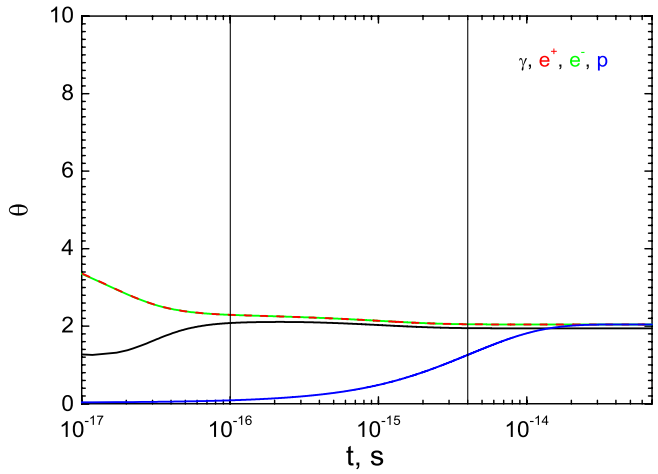

FIG. 14 (color online). Dependence on time of the dimensionless temperature for initial conditions III. Colors are the same as in case I. Pairs and photons acquire the temperature at $t_k \simeq 10^{-16}$ sec.

the vertical line on the right of Figs. 14 and 15. Only at 4×10^{-14} sec do all the particles reach a common temperature equal to $\theta_{th} \simeq 2$, while the chemical potential of protons is $\nu_p \simeq -33$. Initial as well as final spectra are shown in Fig. 16.

Since chemical potentials and temperatures approach their values in thermal equilibrium exponentially, i.e. $\sim \exp(-t/\tau_{ch.eq})$, we determined the relaxation time constant $\tau_{ch.eq}$ for each of the cases considered from

$$\tau_{ch.eq} = \lim_{t\to\infty}\left[(F(t) - F(\infty))\left(\frac{dF}{dt}\right)^{-1}\right], \qquad (24)$$

where the fugacity for a given sort of particle is given by (13). Our results are presented in Table III.

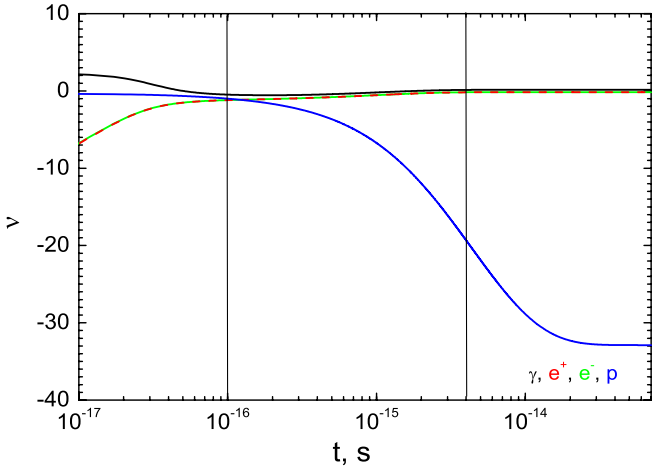

FIG. 15 (color online). Dependence on time of the dimensionless chemical potential for initial conditions III. Colors are the same as in case I. The chemical potentials equalize at $t_k \simeq 10^{-16}$ sec.

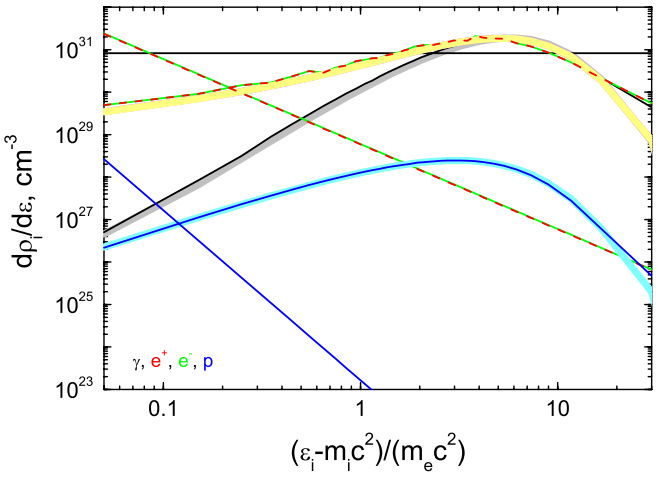

FIG. 16 (color online). Initial and final spectral densities as a function of particle energy for initial conditions III. The spectrum of protons is chosen to be steeper than the one of electrons and positrons. Fits of the final spectra with chemical potentials and temperatures are also shown.

TABLE III. Relaxation time constant for cases I–III.

	I	II	III
$\tau^{\pm,\gamma}_{\mathrm{ch.eq}}$, sec	2.2×10^{-13}	1.8×10^{-14}	9.5×10^{-16}
$\tau^{p}_{\mathrm{ch.eq}}$, sec	6×10^{-13}	1.8×10^{-14}	5.5×10^{-15}

VII. DISCUSSION AND CONCLUSIONS

Results presented above clearly show the existence of two types of equilibrium: kinetic and thermal. Kinetic equilibrium in pair-photon plasma occurs when Ehlers [46] balance conditions (B2), (B5), and (B8) are satisfied so that pair-creation, Compton, and Bhabha/Møller scattering processes all come into detailed balance. The electron-positron-photon plasma is then described by common temperature and nonzero chemical potentials which are given by (B19)–(B22). Protons at this stage may or may not have yet established equilibrium with the spectrum (15), depending on the value of the baryon loading parameter **B**. When **B** is small, as in case I, proton-proton collisions are inefficient since the rate (D15) is much smaller than (D11), and the proton spectrum is shaped by the proton-electron/positron collisions, reaching an equilibrium form at a time scale given by (D11), when other particles are already in thermal equilibrium. When **B** is large, as in case II, protons have established their equilibrium temperature at a time scale given by (D15), prior to the moment when kinetic equilibrium in the pair-photon plasma is established.

As we have seen, the final spectra are completely insensitive to the initial spectra, which are chosen to be flat as in case I, power-law as in case II, or thermal ones.

The meaning of nonzero chemical potentials in kinetic equilibrium can be understood as follows. The existence of a non-null chemical potential for photons indicates the departure of the distribution function from the one corresponding to the thermal equilibrium. Negative values of the chemical potential generate an increase in the number of particles in order to approach the one corresponding to the thermal equilibrium state. Positive values of the chemical potential lead to the opposite effect, decreasing the number of particles. Then, since the total number of particles increases (or decreases), the energy is shared between a larger (or smaller) number of particles and the temperature decreases (or increases). Clearly, as thermal equilibrium is approached, the chemical potential of photons tends to zero, while the chemical potentials of electrons and positrons are given by (B23), to guarantee an overall charge neutrality.

One of the basic assumptions in this work is that triple interactions are slower than binary ones, allowing one to use reaction rates for triple interactions in kinetic equilibrium, explicitly depending solely on temperature, chemical potentials, and concentrations of particles. For pure electron-positron plasma in the range of energies of interest (1), there is a hierarchy of relevant time scales: binary interactions are clearly faster than triple ones. However, when protons are also present, the proton-proton time scale may be shorter or longer than the corresponding binary interaction time scales for the pure pair plasma. This violates our assumption and therefore leads to a loss of quantitative accuracy, although still keeping qualitative results valid. In order to overcome this difficulty and produce quantitatively precise results, exact QED matrix elements must be used for the calculation of emission and absorption coefficients.

Notice that there is some discrepancy between our final spectra and their thermal fits for high energy. This is due to poor energy resolution with the adopted grid. The result converges with higher resolutions, but it is limited by the available computer memory. In addition, the code is quite time-consuming, and the processor time increases with the number of operations as a third power of the number of energy intervals.

In order to resolve proton-electron/positron scattering, the number of energy intervals should be increased as M/m compared to the case of pure pair plasma. Even using an inhomogeneous energy grid with uniform energy steps to the peak of the spectrum $d\rho/d\varepsilon$ and decreasing energy steps as ε^{-1} for higher energies, we have obtained acceptable results with about 10^3 intervals for this reaction. Using such a fine grid is impossible in practice. On the other hand, a small parameter m/M expansion can be adopted. In this way we have introduced the mass scaling, described in Appendix G, which gives quite good accuracy for about 10^2 intervals in energy with an inhomogeneous grid, as described above. Finally, it is important to stress that our code allows for the solution of the Boltzmann equations for long time intervals, with time scales which may differ by

up to 10 orders of magnitude, from electron-positron creation and annihilation processes up to proton-electron/positron scattering (see Fig. 2), unlike approaches based on Monte Carlo techniques [45]. This gives us the possibility to follow the thermalization process until we reach a steady solution, i.e. thermal equilibrium.

The assumption of the constancy of the energy density is only valid if the following three conditions are satisfied:

(i) Plasma is optically thick for photons. This leads to the constraint on the spatial dimensions $R_0 \gg (n_{\rm th}\sigma_T)^{-1} \sim 10^{-5}$ cm.
(ii) Neutrinos are not produced. This gives the constraint on the temperature $\theta \ll 7 \times 10^2$.
(iii) Plasma does not expand. Given $t_{\rm dyn} = (\frac{1}{R}\frac{dR}{dt})^{-1} \gg t_{\rm th}$, this leads to $R_0 \gg 10^{-2}$ cm.

To summarize, we have considered the evolution of initially nonequilibrium optically thick electron-positron-photon plasma with proton loading up to a thermal equilibrium on a time scale $t_{\rm th} \lesssim 10^{-11}$ sec. Starting from arbitrary initial conditions we obtain kinetic equilibrium, on a time scale $t_{\rm k} \lesssim 10^{-14}$ sec, from first principles, solving numerically the relativistic Boltzmann equation with collisional integrals computed from exact QED matrix elements.

The general theoretical framework presented here can be further applied by considering thermalization of different relativistic particles predicted by extensions of the standard model of particle physics with the lepton plasma in the early Universe. The occurrence of the thermalization process of electron-positron plasma in GRBs on a much shorter time scale than the characteristic acceleration time [48] is crucial. Such acceleration time scales are indeed sharply bounded (shorter than 10^3 sec in the laboratory frame). Determination of thermalization time scales as functions of the relevant parameters is important for high-energy plasma physics [49,50]. Finally, these results can, in principle, be tested in laboratory experiments aimed at the generation of electron-positron pairs.

ACKNOWLEDGMENTS

We thank the anonymous referee for comments which improved the presentation of our results.

APPENDIX A: CONSERVATION LAWS

Conservation laws consist of baryon number, charge, and energy conservations. In addition, in binary reactions the particle number is conserved.

The energy conservation law can be rewritten for the spectral density,

$$\frac{d}{dt}\sum_i \rho_i = 0 \quad \text{or} \quad \frac{d}{dt}\sum_{i,\omega} Y_{i,\omega} = 0, \tag{A1}$$

where

$$Y_{i,\omega} = \int_{\epsilon_{i,\omega}-\Delta\epsilon_{i,\omega}/2}^{\epsilon_{i,\omega}+\Delta\epsilon_{i,\omega}/2} E_i d\epsilon. \tag{A2}$$

The particle conservation law in binary reactions gives

$$\frac{d}{dt}\sum_i n_i = 0 \quad \text{or} \quad \frac{d}{dt}\sum_{i,\omega}\frac{Y_{i,\omega}}{\epsilon_{i,\omega}} = 0. \tag{A3}$$

Since baryonic number is conserved, the number density of protons is a constant,

$$\frac{dn_p}{dt} = 0. \tag{A4}$$

For the electrically neutral plasma considered in this paper, charge conservation implies (17).

APPENDIX B: DETERMINATION OF TEMPERATURE AND CHEMICAL POTENTIALS IN KINETIC EQUILIBRIUM

Consider distribution functions for photons and pairs in the most general form (15). If one supposes that the reaction rate for the Bhabha scattering vanishes, i.e. there is equilibrium with respect to the reaction

$$e^+ + e^- \leftrightarrow +e^{+\prime} + e^{-\prime}, \tag{B1}$$

then the corresponding condition can be written in the following way:

$$f_+(1 - f_+{}')f_-(1 - f_-{}') = f_+{}'(1 - f_+)f_-{}'(1 + f_-), \tag{B2}$$

where the Bose-Einstein enhancement and the Pauli blocking factors are included for generality; it can be shown that electrons and positrons have the same temperature,

$$\theta_+ = \theta_- \equiv \theta_\pm, \tag{B3}$$

and that they have arbitrary chemical potentials. With (B3) an analogous consideration for the Compton scattering,

$$e^\pm + \gamma \leftrightarrow +e^{\pm\prime} + \gamma', \tag{B4}$$

gives

$$f_\pm(1 - f_\pm{}')f_\gamma(1 + f_\gamma{}') = f_\pm{}'(1 - f_\pm)f_\gamma{}'(1 + f_\gamma), \tag{B5}$$

and leads to the equality of temperatures of pairs and photons,

$$\theta_\pm = \theta_\gamma \equiv \theta_k, \tag{B6}$$

with arbitrary chemical potentials. If, in addition, the reaction rate in the pair-creation and annihilation process

$$e^\pm + e^\mp \leftrightarrow \gamma + \gamma' \tag{B7}$$

vanishes too, i.e. there is equilibrium with respect to pair production and annihilation, with the corresponding condition

$$f_+ f_-(1+f_\gamma)(1+f_\gamma{}') = f_\gamma f_\gamma{}'(1-f_+)(1-f_-), \tag{B8}$$

it turns out that chemical potentials of pairs and photons also satisfy the following condition:

$$\nu_+ + \nu_- = 2\nu_\gamma. \tag{B9}$$

However, since, generally speaking, $\nu_\gamma \neq 0$, the condition (B9) does not imply $\nu_+ = \nu_-$. These conditions were applied for the first time by Ehlers in [46] (see also [51]), and we will call (B2), (B5), and (B8) the *Ehlers balance conditions*.

Analogous conditions for the detailed balance conditions in different reactions lead to relations between temperatures and chemical potentials as summarized in Table IV.

The time scales of pair production and annihilation processes as well as Compton scattering are nearly equal in the range of energies of interest and are given by (14). Therefore, kinetic equilibrium is first established simultaneously for electrons, positrons, and photons. They reach the same temperature, but with chemical potentials different from zero. Later on, the temperatures of this electron-positron-photon plasma and the one of protons reach a common value.

In order to find temperatures and chemical potentials, we have to implement the following constraints: energy conservation (A1), particle number conservation (A3), charge conservation (17), and the condition for the chemical potentials (B9).

Given (15) we have for photons

$$\frac{\rho_\gamma}{n_\gamma mc^2} = 3\theta_\gamma, \qquad n_\gamma = \frac{1}{V_0}\exp\left(\frac{\nu_\gamma}{\theta_\gamma}\right)2\theta_\gamma^3, \tag{B10}$$

for pairs

$$\frac{\rho_\pm}{n_\pm mc^2} = j_2(\theta_\pm), \qquad n_\pm = \frac{1}{V_0}\exp\left(\frac{\nu_\pm}{\theta_\pm}\right)j_1(\theta_\pm), \tag{B11}$$

and for protons

$$\frac{\rho_p}{Mn_pc^2} = 1 + \frac{3}{2}\frac{m}{M}\theta_p, \tag{B12}$$

TABLE IV. Relations between the parameters of equilibrium distribution functions fulfilling detailed balance conditions for the reactions shown in Table I.

	Interaction	Parameters
I	e^+e^- scattering	$\theta_+ = \theta_-$, $\forall\ \nu_+, \nu_-$
II	$e^\pm p$ scattering	$\theta_p = \theta_\pm$, $\forall\ \nu_\pm, \nu_p$
III	$e^\pm\gamma$ scattering	$\theta_\gamma = \theta_\pm$, $\forall\ \nu_\gamma, \nu_\pm$
IV	Pair production	$\nu_+ + \nu_- = 2\nu_\gamma$, if $\theta_\gamma = \theta_\pm$
V	Tripe interactions	$\nu_\gamma, \nu_\pm = 0$, if $\theta_\gamma = \theta_\pm$

$$n_p = \frac{1}{V_0}\sqrt{\frac{\pi}{2}}\left(\frac{M}{m}\right)^{3/2}\exp\left(\frac{\nu_p - \frac{M}{m}}{\theta_p}\right)\theta_p^{3/2}, \tag{B13}$$

where we assumed that protons are nonrelativistic; we denoted the Compton volume by

$$V_0 = \frac{1}{8\pi}\left(\frac{2\pi\hbar}{mc}\right)^3, \tag{B14}$$

and functions j_1 and j_2 are defined as

$$j_1(\theta) = \theta K_2(\theta^{-1}) \to \begin{cases} \sqrt{\frac{\pi}{2}}e^{-(1/\theta)}\theta^{3/2} & \theta \to 0 \\ 2\theta^3 & \theta \to \infty, \end{cases} \tag{B15}$$

$$j_2(\theta) = \frac{3K_3(\theta^{-1}) + K_1(\theta^{-1})}{4K_2(\theta^{-1})} \to \begin{cases} 1 + \frac{3\theta}{2} & \theta \to 0 \\ 3\theta & \theta \to \infty. \end{cases} \tag{B16}$$

For pure electron-positron-photon plasma in kinetic equilibrium, summing up energy densities in (B10) and (B11) and using (B3), (B6), and (B9), we obtain

$$\sum_{e^+,e^-,\gamma}\rho_i = \frac{2mc^2}{V_0}\exp\left(\frac{\nu_k}{\theta_k}\right)[3\theta^4 + j_1(\theta_k)j_2(\theta_k)], \tag{B17}$$

and analogously for number densities we get

$$\sum_{e^+,e^-,\gamma} n_i = \frac{2}{V_0}\exp\left(\frac{\nu_k}{\theta_k}\right)[\theta_k^3 + j_1(\theta_k)]. \tag{B18}$$

From (B17) and (B18) two unknowns, ν_k and θ_k, can be found.

When protons are present, in most cases the electron-positron-photon plasma reaches kinetic equilibrium first, while protons join the plasma later. In that case, the temperature of protons θ_p is different from the rest of the particles, so while $\theta_+ = \theta_- = \theta_\gamma = \theta_k$, $\theta_p \neq \theta_k$.

Then, summing up energy densities in (B10) and (B11) we obtain

$$\sum_{e^+,e^-,\gamma}\rho_i = \frac{mc^2}{V_0}\left\{\left[1 - \frac{n_pV_0}{j_1(\theta_k)}\exp\left(-\frac{\nu_+}{\theta_k}\right)\right]^{1/2}6\theta_k^4\exp\left(\frac{\nu_+}{\theta_k}\right) + \left[2j_1(\theta_k)\exp\left(\frac{\nu_+}{\theta_k}\right) - n_pV_0\right]j_2(\theta_k)\right\}, \tag{B19}$$

and analogously for number densities we get

$$\sum_{e^+,e^-,\gamma} n_i = \frac{1}{V_0}\left\{\left[1 - \frac{n_pV_0}{j_1(\theta_k)}\exp\left(-\frac{\nu_+}{\theta_k}\right)\right]^{1/2}6\theta_k^4\exp\left(\frac{\nu_+}{\theta_k}\right) + 2j_1(\theta_k)\exp\left(\frac{\nu_+}{\theta_k}\right)\right\}. \tag{B20}$$

From (B19) and (B20) two unknowns, ν_+ and θ_k, can be found. Then the rest of the chemical potentials are obtained from

$$\exp\left(\frac{\nu_-}{\theta_k}\right) = \exp\left(\frac{\nu_+}{\theta_k}\right) + \frac{n_pV_0}{j_1(\theta_k)}, \tag{B21}$$

$$\exp\left(\frac{\nu_\gamma}{\theta_k}\right) = \exp\left(\frac{\nu_+}{\theta_k}\right)\left[1 + \frac{n_p V_0}{j_1(\theta_k)} \exp\left(-\frac{\nu_+}{\theta_k}\right)\right]^{1/2}. \tag{B22}$$

The temperature and chemical potential of protons can be found separately from (B12) and (B13).

In thermal equilibrium ν_γ vanishes and one has

$$\nu_- = \theta_k \mathrm{arcsinh}\left[\frac{n_p V_0}{2 j_1(\theta_k)}\right], \qquad \nu_+ = -\nu_-, \tag{B23}$$

which both reduce to $\nu_- = \nu_+ = 0$ for $n_p = 0$. At the same time, for $n_p > 0$ one always has $\nu_- > 0$ and $\nu_+ < 0$ in thermal equilibrium. The chemical potential of protons in thermal equilibrium is determined from (B13) for $\theta_k = \theta_{th}$, where θ_{th} is the temperature in thermal equilibrium.

APPENDIX C: BINARY INTERACTIONS

1. Compton scattering, $\gamma e^\pm \to \gamma' e^{\pm\prime}$

The time evolution of the distribution functions of photons and pair particles due to Compton scattering may be described by [33,52]

$$\left(\frac{\partial f_\gamma(\mathbf{k},t)}{\partial t}\right)_{\gamma e^\pm \to \gamma' e^{\pm\prime}} = \int d\mathbf{k}' d\mathbf{p} d\mathbf{p}' V w_{\mathbf{k}',\mathbf{p}';\mathbf{k},\mathbf{p}} [f_\gamma(\mathbf{k}',t) \times f_\pm(\mathbf{p}',t) - f_\gamma(\mathbf{k},t) f_\pm(\mathbf{p},t)], \tag{C1}$$

$$\left(\frac{\partial f_\pm(\mathbf{p},t)}{\partial t}\right)_{\gamma e^\pm \to \gamma' e^{\pm\prime}} = \int d\mathbf{k} d\mathbf{k}' d\mathbf{p}' V w_{\mathbf{k}',\mathbf{p}';\mathbf{k},\mathbf{p}} [f_\gamma(\mathbf{k}',t) \times f_\pm(\mathbf{p}',t) - f_\gamma(\mathbf{k},t) f_\pm(\mathbf{p},t)], \tag{C2}$$

where

$$w_{\mathbf{k}',\mathbf{p}';\mathbf{k},\mathbf{p}} = \frac{\hbar^2 c^6}{(2\pi)^2 V} \delta(\epsilon_\gamma - \epsilon_\pm - \epsilon'_\gamma - \epsilon'_\pm) \times \delta(\mathbf{k} + \mathbf{p} - \mathbf{k}' - \mathbf{p}') \frac{|M_{fi}|^2}{16 \epsilon_\gamma \epsilon_\pm \epsilon'_\gamma \epsilon'_\pm} \tag{C3}$$

is the probability of the process,

$$|M_{fi}|^2 = 2^6 \pi^2 \alpha^2 \left[\frac{m^2c^2}{s - m^2c^2} + \frac{m^2c^2}{u - m^2c^2} + \left(\frac{m^2c^2}{s - m^2c^2} + \frac{m^2c^2}{u - m^2c^2}\right)^2 - \frac{1}{4}\left(\frac{s - m^2c^2}{u - m^2c^2} + \frac{u - m^2c^2}{s - m^2c^2}\right)\right] \tag{C4}$$

is the square of the matrix element, $s = (\mathfrak{p} + \mathfrak{k})^2$ and $u = (\mathfrak{p} - \mathfrak{k}')^2$ are invariants, $\mathfrak{k} = (\epsilon_\gamma/c)(1, \mathbf{e}_\gamma)$ and $\mathfrak{p} = (\epsilon_\pm/c)(1, \beta_\pm \mathbf{e}_\pm)$ are energy-momentum four-vectors of photons and electrons, respectively, $d\mathbf{p} = d\epsilon_\pm do \epsilon_\pm^2 \beta_\pm / c^3$, $d\mathbf{k}' = d\epsilon'_\gamma \epsilon'^2_\gamma do'_\gamma / c^3$, and $do = d\mu d\phi$.

The energies of the photon and the positron (electron) after the scattering are

$$\epsilon'_\gamma = \frac{\epsilon_\pm \epsilon_\gamma (1 - \beta_\pm \mathbf{b}_\pm \cdot \mathbf{b}_\gamma)}{\epsilon_\pm (1 - \beta_\pm \mathbf{b}_\pm \cdot \mathbf{b}'_\gamma) + \epsilon_\gamma (1 - \mathbf{b}_\gamma \cdot \mathbf{b}'_\gamma)}, \qquad \epsilon'_\pm = \epsilon_\pm + \epsilon_\gamma - \epsilon'_\gamma, \tag{C5}$$

$\mathbf{b}_i = \mathbf{p}_i/p$, $\mathbf{b}'_i = \mathbf{p}'_i/p'$, $\mathbf{b}'_\pm = (\beta_\pm \epsilon_\pm \mathbf{b}_\pm + \epsilon_\gamma \mathbf{b}_\gamma - \epsilon'_\gamma \mathbf{b}'_\gamma)/(\beta'_\pm \epsilon'_\pm)$.

For photons, the absorption coefficient (10) in the Boltzmann equations (4) is

$$\chi_\gamma^{\gamma e^\pm \to \gamma' e^{\pm\prime}} f_\gamma = -\frac{1}{c}\left(\frac{\partial f_\gamma}{\partial t}\right)^{\mathrm{abs}}_{\gamma e^\pm \to \gamma' e^{\pm\prime}} = \int dn_\pm do'_\gamma J_{cs} \frac{\epsilon'_\gamma |M_{fi}|^2 \hbar^2 c^2}{16 \epsilon_\pm \epsilon_\gamma \epsilon'_\pm} f_\gamma, \tag{C6}$$

where $dn_i = d\epsilon_i do_i \epsilon_i^2 \beta_i f_i / c^3 = d\epsilon_i do_i E_i / (2\pi \epsilon_i)$.

From Eqs. (C1) and (C6), we can write the absorption coefficient for the photon energy density E_γ averaged over the ϵ, μ grid with zone numbers ω and k as

$$(\chi E)^{\gamma e^\pm \to \gamma' e^{\pm\prime}}_{\gamma,\omega} \equiv \frac{1}{\Delta \epsilon_{\gamma,\omega}} \int_{\epsilon_\gamma \in \Delta \epsilon_{\gamma,\omega}} d\epsilon_\gamma d\mu_\gamma (\chi E)^{\gamma e^\pm \to \gamma' e^{\pm\prime}}_\gamma = \frac{1}{\Delta \epsilon_{\gamma,\omega}} \int_{\epsilon_\gamma \in \Delta \epsilon_{\gamma,\omega}} dn_\gamma dn_\pm do'_\gamma J_{cs} \times \frac{\epsilon'_\gamma |M_{fi}|^2 \hbar^2 c^2}{16 \epsilon_\pm \epsilon'_\pm}, \tag{C7}$$

where the Jacobian of the transformation is

$$J_{cs} = \frac{\epsilon'_\gamma \epsilon'_\pm}{\epsilon_\gamma \epsilon_\pm (1 - \beta_\pm \mathbf{b}_\gamma \cdot \mathbf{b}_\pm)}. \tag{C8}$$

Similar integrations can be performed for the other terms of Eqs. (C1) and (C2), and we obtain

$$\eta^{\gamma e^\pm \to \gamma' e^{\pm\prime}}_{\gamma,\omega} = \frac{1}{\Delta \epsilon_{\gamma,\omega}} \int_{\epsilon'_\gamma \in \Delta \epsilon_{\gamma,\omega}} dn_\gamma dn_\pm do'_\gamma J_{cs} \times \frac{\epsilon'^2_\gamma |M_{fi}|^2 \hbar^2 c^2}{16 \epsilon_\pm \epsilon_\gamma \epsilon'_\pm}, \tag{C9}$$

$$\eta^{\gamma e^\pm \to \gamma' e^{\pm\prime}}_{\pm,\omega} = \frac{1}{\Delta \epsilon_{\pm,\omega}} \int_{\epsilon'_\pm \in \Delta \epsilon_{\pm,\omega}} dn_\gamma dn_\pm do'_\gamma J_{cs} \times \frac{\epsilon'_\gamma |M_{fi}|^2 \hbar^2 c^2}{16 \epsilon_\pm \epsilon_\gamma}, \tag{C10}$$

$$(\chi E)^{\gamma e^\pm \to \gamma' e^{\pm\prime}}_{\pm,\omega} = \frac{1}{\Delta \epsilon_{\pm,\omega}} \int_{\epsilon_\pm \in \Delta \epsilon_{\pm,\omega}} dn_\gamma dn_\pm do'_\gamma J_{cs} \times \frac{\epsilon'_\gamma |M_{fi}|^2 \hbar^2 c^2}{16 \epsilon_\gamma \epsilon'_\pm}. \tag{C11}$$

In order to perform integrals (C7)–(C11) numerically over ϕ ($0 \le \phi \le 2\pi$), we introduce a uniform grid $\phi_{l\mp 1/2}$ with $1 \le l \le l_{\max}$ and $\Delta\phi_l = (\phi_{l+1/2} - \phi_{l-1/2})/2 = 2\pi/l_{\max}$. We assume that any function of ϕ in Eqs. (C7)–(C9) in the interval $\Delta\phi_j$ is equal to its value at $\phi = \phi_j = (\phi_{l-1/2} + \phi_{l+1/2})/2$. It is necessary to integrate over ϕ only once at the beginning of the calculations. The number of intervals of the ϕ grid depends on the average energy of particles and is typically taken as $l_{\max} = 2k_{\max} = 64$.

2. Pair creation and annihilation, $\gamma_1\gamma_2 \rightleftarrows e^- e^+$

The rates of change of the distribution function due to pair creation and annihilation are

$$\left(\frac{\partial f_{\gamma_j}(\mathbf{k}_j, t)}{\partial t}\right)_{\gamma_1\gamma_2 \to e^- e^+} = -\int d\mathbf{k}_j d\mathbf{p}_- d\mathbf{p}_+ V w_{\mathbf{p}_-,\mathbf{p}_+;\mathbf{k}_1,\mathbf{k}_2} \times f_{\gamma_1}(\mathbf{k}_1, t) f_{\gamma_2}(\mathbf{k}_2, t), \tag{C12}$$

$$\left(\frac{\partial f_{\gamma_i}(\mathbf{k}_i, t)}{\partial t}\right)_{e^- e^+ \to \gamma_1\gamma_2} = \int d\mathbf{k}_j d\mathbf{p}_- d\mathbf{p}_+ V w_{\mathbf{k}_1,\mathbf{k}_2;\mathbf{p}_-,\mathbf{p}_+} \times f_-(\mathbf{p}_-, t) f_+(\mathbf{p}_+, t), \tag{C13}$$

for $i = 1$, $j = 2$, and for $j = 1$, $i = 2$.

$$\left(\frac{\partial f_{\pm}(\mathbf{p}_{\pm}, t)}{\partial t}\right)_{\gamma_1\gamma_2 \to e^- e^+} = \int d\mathbf{p}_{\mp} d\mathbf{k}_1 d\mathbf{k}_2 V w_{\mathbf{p}_-,\mathbf{p}_+;\mathbf{k}_1,\mathbf{k}_2} \times f_\gamma(\mathbf{k}_1, t) f_\gamma(\mathbf{k}_2, t), \tag{C14}$$

$$\left(\frac{\partial f_{\pm}(\mathbf{p}_{\pm}, t)}{\partial t}\right)_{e^- e^+ \to \gamma_1\gamma_2} = -\int d\mathbf{p}_{\mp} d\mathbf{k}_1 d\mathbf{k}_2 V w_{\mathbf{k}_1,\mathbf{k}_2;\mathbf{p}_-,\mathbf{p}_+} \times f_-(\mathbf{p}_-, t) f_+(\mathbf{p}_+, t), \tag{C15}$$

where

$$w_{\mathbf{p}_-,\mathbf{p}_+;\mathbf{k}_1,\mathbf{k}_2} = \frac{\hbar^2 c^6}{(2\pi)^2 V}\delta(\epsilon_- + \epsilon_+ - \epsilon_1 - \epsilon_2) \times \delta(\mathbf{p}_- + \mathbf{p}_+ - \mathbf{k}_1 - \mathbf{k}_2)\frac{|M_{fi}|^2}{16\epsilon_-\epsilon_+\epsilon_1\epsilon_2}. \tag{C16}$$

Here, the matrix element $|M_{fi}|^2$ is given by Eq. (C4) with the new invariants $s = (\mathfrak{p}_- - \mathfrak{k}_1)^2$ and $u = (\mathfrak{p}_- - \mathfrak{k}_2)^2$; see [41].

The energies of photons created via annihilation of an $e^{\pm}$ pair are

$$\epsilon_1(\mathbf{b}_1) = \frac{m^2c^4 + \epsilon_-\epsilon_+(1 - \beta_-\beta_+\mathbf{b}_-\cdot\mathbf{b}_+)}{\epsilon_-(1 - \beta_-\mathbf{b}_-\cdot\mathbf{b}_1) + \epsilon_+(1 - \beta_+\mathbf{b}_+\cdot\mathbf{b}_1)},$$
$$\epsilon_2(\mathbf{b}_1) = \epsilon_- + \epsilon_+ - \epsilon_1, \tag{C17}$$

while the energies of pair particles created by two photons are found from

$$\epsilon_-(\mathbf{b}_-) = \frac{B \mp \sqrt{B^2 - AC}}{A},$$
$$\epsilon_+(\mathbf{b}_-) = \epsilon_1 + \epsilon_2 - \epsilon_-, \tag{C18}$$

where $A = (\epsilon_1 + \epsilon_2)^2 - [(\epsilon_1\mathbf{b}_1 + \epsilon_2\mathbf{b}_2)\cdot\mathbf{b}_-]^2$, $B = (\epsilon_1 + \epsilon_2)\epsilon_1\epsilon_2(1 - \mathbf{b}_1\cdot\mathbf{b}_2)$, $C = m_e^2c^4[(\epsilon_1\mathbf{b}_1 + \epsilon_2\mathbf{b}_2)\cdot\mathbf{b}_-]^2 + \epsilon_1^2\epsilon_2^2(1 - \mathbf{b}_1\cdot\mathbf{b}_2)^2$. Only one root in Eq. (C18) has to be chosen. Energy-momentum conservation gives

$$\mathfrak{k}_1 + \mathfrak{k}_2 - \mathfrak{p}_- = \mathfrak{p}_+. \tag{C19}$$

Taking the square from the energy part, we have

$$\epsilon_1^2 + \epsilon_2^2 + \epsilon_-^2 + 2\epsilon_1\epsilon_2 - 2\epsilon_1\epsilon_- - 2\epsilon_2\epsilon_- = \epsilon_+^2, \tag{C20}$$

and taking the square from the momentum part, we get

$$\epsilon_1^2 + \epsilon_2^2 + \epsilon_-^2\beta_-^2 + 2\epsilon_1\epsilon_2\mathbf{b}_1\cdot\mathbf{b}_2 - 2\epsilon_1\epsilon_-\beta_-\mathbf{b}_1\cdot\mathbf{b}_- - 2\epsilon_2\epsilon_-\beta_-\mathbf{b}_2\cdot\mathbf{b}_- = (\epsilon_+\beta_+)^2. \tag{C21}$$

There are no additional roots because of the arbitrary $\mathbf{e}_+$,

$$\epsilon_1\epsilon_2(1 - \mathbf{b}_1\cdot\mathbf{b}_2) - \epsilon_1\epsilon_-(1 - \beta_-\mathbf{b}_1\cdot\mathbf{b}_-) - \epsilon_2\epsilon_-(1 - \beta\mathbf{b}_2\cdot\mathbf{b}_-) = 0,$$
$$\epsilon_-\beta_-(\epsilon_1\mathbf{b}_1 + \epsilon_2\mathbf{b}_2)\cdot\mathbf{b}_- = \epsilon_-(\epsilon_1 + \epsilon_2) - \epsilon_1\epsilon_2(1 - \mathbf{b}_1\cdot\mathbf{b}_2). \tag{C22}$$

Eliminating β we obtain

$$\epsilon_1^2\epsilon_2^2(1 - \mathbf{b}_1\cdot\mathbf{b}_2)^2 - 2\epsilon_1\epsilon_2(1 - \mathbf{b}_1\cdot\mathbf{b}_2)(\epsilon_1 + \epsilon_2)\epsilon_- + \{(\epsilon_1 + \epsilon_2)^2 - [(\epsilon_1\mathbf{b}_1 + \epsilon_2\mathbf{b}_2)\cdot\mathbf{b}_-]^2\}\epsilon_-^2 = [(\epsilon_1\mathbf{b}_1 + \epsilon_2\mathbf{b}_2)\cdot\mathbf{b}_-](-m^2). \tag{C23}$$

Therefore, the condition to be checked reads

$$\epsilon_-\beta_-[(\epsilon_1\mathbf{b}_1+\epsilon_2\mathbf{b}_2)\cdot\mathbf{b}_-]^2 = [\epsilon_-(\epsilon_1+\epsilon_2)-(\epsilon_1\epsilon_2)(1-\mathbf{b}_1\cdot\mathbf{b}_2)] \times[(\epsilon_1\mathbf{b}_1+\epsilon_2\mathbf{b}_2)\cdot\mathbf{b}_-]\geq 0. \quad \text{(C24)}$$

Finally, integration of Eqs. (C12)–(C15) yields

$$\eta^{e^-e^+\to\gamma_1\gamma_2}_{\gamma,\omega} = \frac{1}{\Delta\epsilon_{\gamma,\omega}}\left(\int_{\epsilon_1\in\Delta\epsilon_{\gamma,\omega}} d^2n_\pm J_{\rm ca}\frac{\epsilon_1^2|M_{fi}|^2\hbar^2c^2}{16\epsilon_-\epsilon_+\epsilon_2} + \int_{\epsilon_2\in\Delta\epsilon_{\gamma,\omega}} d^2n_\pm J_{\rm ca}\frac{\epsilon_1|M_{fi}|^2\hbar^2c^2}{16\epsilon_-\epsilon_+}\right), \quad \text{(C25)}$$

$$(\chi E)^{e^-e^+\to\gamma_1\gamma_2}_{e,\omega} = \frac{1}{\Delta\epsilon_{e,\omega}}\left(\int_{\epsilon_-\in\Delta\epsilon_{e,\omega}} d^2n_\pm J_{\rm ca}\frac{\epsilon_1|M_{fi}|^2\hbar^2c^2}{16\epsilon_+\epsilon_2} + \int_{\epsilon_+\in\Delta\epsilon_{e,\omega}} d^2n_\pm J_{\rm ca}\frac{\epsilon_1|M_{fi}|^2\hbar^2c^2}{16\epsilon_-\epsilon_2}\right), \quad \text{(C26)}$$

$$(\chi E)^{\gamma_1\gamma_2\to e^-e^+}_{\gamma,\omega} = \frac{1}{\Delta\epsilon_{\gamma,\omega}}\left(\int_{\epsilon_1\in\Delta\epsilon_{\gamma,\omega}} d^2n_\gamma J_{\rm ca}\frac{\epsilon_-\beta_-|M_{fi}|^2\hbar^2c^2}{16\epsilon_2\epsilon_+} + \int_{\epsilon_2\in\Delta\epsilon_{\gamma,\omega}} d^2n_\gamma J_{\rm ca}\frac{\epsilon_-\beta_-|M_{fi}|^2\hbar^2c^2}{16\epsilon_1\epsilon_+}\right), \quad \text{(C27)}$$

$$\eta^{\gamma_1\gamma_2\to e^-e^+}_{e,\omega} = \frac{1}{\Delta\epsilon_{e,\omega}}\left(\int_{\epsilon_-\in\Delta\epsilon_{e,\omega}} d^2n_\gamma J_{\rm ca}\frac{\epsilon_-^2\beta_-|M_{fi}|^2\hbar^2c^2}{16\epsilon_1\epsilon_2\epsilon_+} + \int_{\epsilon_+\in\Delta\epsilon_{e,\omega}} d^2n_\gamma J_{\rm ca}\frac{\epsilon_-\beta_-|M_{fi}|^2\hbar^2c^2}{16\epsilon_1\epsilon_2}\right), \quad \text{(C28)}$$

where $d^2n_\pm = dn_-dn_+do_1$, $d^2n_\gamma = dn_{\gamma_1}dn_{\gamma_2}do_-$, $dn_\pm = d\epsilon_\pm do_\pm\epsilon_\pm^2\beta_\pm f_\pm$, $dn_{\gamma_{1,2}} = d\epsilon_{1,2}do_{1,2}\epsilon_{1,2}^2 f_{\gamma_{1,2}}$, and the Jacobian is

$$J_{\rm ca} = \frac{\epsilon_+\beta_-}{(\epsilon_++\epsilon_-)\beta_- - (\epsilon_1\mathbf{b}_1+\epsilon_2\mathbf{b}_2)\cdot\mathbf{b}_-}. \quad \text{(C29)}$$

3. Møller scattering of electrons and positrons, $e_1^\pm e_2^\pm \to e_1^{\pm\prime} e_2^{\pm\prime}$

The time evolution of the distribution functions of electrons (or positrons) is described by

$$\left(\frac{\partial f_i(\mathbf{p}_i,t)}{\partial t}\right)_{e_1e_2\to e_1'e_2'} = \int d\mathbf{p}_j d\mathbf{p}_1' d\mathbf{p}_2' V w_{\mathbf{p}_1',\mathbf{p}_2';\mathbf{p}_1,\mathbf{p}_2}[f_1(\mathbf{p}_1',t) \times f_2(\mathbf{p}_2',t) - f_1(\mathbf{p}_1,t)f_2(\mathbf{p}_2,t)], \quad \text{(C30)}$$

with $i=1$, $j=2$, and with $j=1$, $i=2$, and where

$$w_{\mathbf{p}_1',\mathbf{p}_2';\mathbf{p}_1,\mathbf{p}_2} = \frac{\hbar^2c^6}{(2\pi)^2V}\delta(\epsilon_1+\epsilon_2-\epsilon_1'-\epsilon_2') \times\delta(\mathbf{p}_1+\mathbf{p}_2-\mathbf{p}_1'-\mathbf{p}_2')\frac{|M_{fi}|^2}{16\epsilon_1\epsilon_2\epsilon_1'\epsilon_2'}, \quad \text{(C31)}$$

$$|M_{fi}|^2 = 2^6\pi^2\alpha^2\left\{\frac{1}{t^2}\left[\frac{s^2+u^2}{2}+4m^2c^2(t-m^2c^2)\right] + \frac{1}{u^2}\left[\frac{s^2+t^2}{2}+4m^2c^2(u-m^2c^2)\right] + \frac{4}{tu}\left(\frac{s}{2}-m^2c^2\right)\left(\frac{s}{2}-3m^2c^2\right)\right\}, \quad \text{(C32)}$$

with $s=(\mathfrak{p}_1+\mathfrak{p}_2)^2 = 2(m^2c^2+\mathfrak{p}_1\mathfrak{p}_2)$, $t=(\mathfrak{p}_1-\mathfrak{p}_1')^2 = 2(m^2c^2-\mathfrak{p}_1\mathfrak{p}_1')$, and $u=(\mathfrak{p}_1-\mathfrak{p}_2')^2 = 2(m^2c^2-\mathfrak{p}_1\mathfrak{p}_2')$ [41].

The energies of final-state particles are given by (C18) with new coefficients $\tilde{A} = (\epsilon_1+\epsilon_2)^2 - (\epsilon_1\beta_1\mathbf{b}_1\cdot\mathbf{b}_1' + \epsilon_2\beta_2\mathbf{b}_2\cdot\mathbf{b}_1')^2$, $\tilde{B} = (\epsilon_1+\epsilon_2)[m^2c^4+\epsilon_1\epsilon_2(1-\beta_1\beta_2\mathbf{b}_1\mathbf{b}_2)]$, and $\tilde{C} = m^2c^4(\epsilon_1\beta_1\mathbf{b}_1\cdot\mathbf{b}_1' + \epsilon_2\beta_2\mathbf{b}_2\cdot\mathbf{b}_1')^2 + [m^2c^4+\epsilon_1\epsilon_2(1-\beta_1\beta_2\mathbf{b}_1\cdot\mathbf{b}_2)]^2$. The condition to be checked is

$$[\epsilon_1'(\epsilon_1+\epsilon_2) - m^2c^4 - (\epsilon_1\epsilon_2)(1-\beta_1\beta_2\mathbf{b}_1\cdot\mathbf{b}_2)] \times[(\epsilon_1\beta_1\mathbf{b}_1+\epsilon_2\beta_2\mathbf{b}_2)\cdot\mathbf{b}_1'] \geq 0. \quad \text{(C33)}$$

Integration of Eqs. (C30), similar to the case of Compton scattering in Sec. C 1, yields

$$\eta^{e_1e_2\to e_1'e_2'}_{e,\omega} = \frac{1}{\Delta\epsilon_{e,\omega}}\left(\int_{\epsilon_1'\in\Delta\epsilon_{e,\omega}} d^2nJ_{\rm ms}\frac{\epsilon_1'^2\beta_1'|M_{fi}|^2\hbar^2c^2}{16\epsilon_1\epsilon_2\epsilon_2'} + \int_{\epsilon_2'\in\Delta\epsilon_{e,\omega}} d^2nJ_{\rm ms}\frac{\epsilon_1'\beta_1'|M_{fi}|^2\hbar^2c^2}{16\epsilon_1\epsilon_2}\right), \quad \text{(C34)}$$

$$(\chi E)^{e_1e_2\to e_1'e_2'}_{e,\omega} = \frac{1}{\Delta\epsilon_{e,\omega}}\left(\int_{\epsilon_1\in\Delta\epsilon_{e,\omega}} d^2nJ_{\rm ms}\frac{\epsilon_1'\beta_1'|M_{fi}|^2\hbar^2c^2}{16\epsilon_2\epsilon_2'} + \int_{\epsilon_2\in\Delta\epsilon_{e,\omega}} d^2nJ_{\rm ms}\frac{\epsilon_1'\beta_1'|M_{fi}|^2\hbar^2c^2}{16\epsilon_1\epsilon_2'}\right), \quad \text{(C35)}$$

where $d^2n = dn_1dn_2do_1'$, $dn_{1,2} = d\epsilon_{1,2}do_{1,2}\epsilon_{1,2}^2\beta_{1,2}f_{1,2}$, and the Jacobian is

$$J_{\rm ms} = \frac{\epsilon_2'\beta_2'}{(\epsilon_1'+\epsilon_2')\beta_1' - (\epsilon_1\beta_1\mathbf{b}_1+\epsilon_2\beta_2\mathbf{b}_2)\cdot\mathbf{b}_1'}. \quad \text{(C36)}$$

4. Bhabha scattering of electrons on positrons, $e^-e^+ \to e^{-\prime}e^{+\prime}$

The time evolution of the distribution functions of electrons and positrons due to Bhabha scattering is described by

$$\left(\frac{\partial f_\pm(\mathbf{p}_\pm,t)}{\partial t}\right)_{e^-e^+\to e^{-\prime}e^{+\prime}} = \int d\mathbf{p}_\mp d\mathbf{p}'_- d\mathbf{p}'_+ V w_{\mathbf{p}'_-,\mathbf{p}'_+;\mathbf{p}_-,\mathbf{p}_+} \times [f_-(\mathbf{p}'_-,t) f_+(\mathbf{p}'_+,t) - f_-(\mathbf{p}_-,t) f_+(\mathbf{p}_+,t)], \quad \text{(C37)}$$

where

$$w_{\mathbf{p}'_-,\mathbf{p}'_+;\mathbf{p}_-,\mathbf{p}_+} = \frac{\hbar^2 c^6}{(2\pi)^2 V}\delta(\epsilon_- + \epsilon_+ - \epsilon'_- - \epsilon'_+) \times \delta(\mathbf{p}_- + \mathbf{p}_+ - \mathbf{p}'_- - \mathbf{p}'_+)\frac{|M_{fi}|^2}{16\epsilon_-\epsilon_+\epsilon'_-\epsilon'_+}, \quad \text{(C38)}$$

and $|M_{fi}|$ is given by Eq. (C32), but the invariants are $s = (\mathfrak{p}_- - \mathfrak{p}'_+)^2$, $t = (\mathfrak{p}_+ - \mathfrak{p}'_+)^2$, and $u = (\mathfrak{p}_- + \mathfrak{p}_+)^2$. The final energies ϵ'_-, ϵ'_+ are functions of the outgoing particle directions in a way similar to that in Sec. C 3; see also [41].

Integration of Eqs. (C37) yields

$$\eta^{e^-e^+\to e^{-\prime}e^{+\prime}}_{\pm,\omega} = \frac{1}{\Delta\epsilon_{\pm,\omega}}\left(\int_{\epsilon'_-\in\Delta\epsilon_{e,\omega}} d^2n'_\pm J_{\rm bs} \times \frac{\epsilon'^2_- \beta'_- |M_{fi}|^2\hbar^2c^2}{16\epsilon_-\epsilon_+\epsilon'_+} + \int_{\epsilon'_+\in\Delta\epsilon_{e,\omega}} d^2n'_\pm J_{\rm bs} \times \frac{\epsilon'_-\beta'_-|M_{fi}|^2\hbar^2c^2}{16\epsilon_-\epsilon_+}\right), \quad \text{(C39)}$$

$$(\chi E)^{e^-e^+\to e^{-\prime}e^{+\prime}}_{\pm,\omega} = \frac{1}{\Delta\epsilon_{\pm,\omega}}\left(\int_{\epsilon_-\in\Delta\epsilon_{e,\omega}} d^2n'_\pm J_{\rm bs} \times \frac{\epsilon'_-\beta'_-|M_{fi}|^2\hbar^2c^2}{16\epsilon_+\epsilon'_+} + \int_{\epsilon_+\in\Delta\epsilon_{e,\omega}} d^2n'_\pm J_{\rm bs} \times \frac{\epsilon'_-\beta'_-|M_{fi}|^2\hbar^2c^2}{16\epsilon_-\epsilon'_+}\right), \quad \text{(C40)}$$

where $d^2n'_\pm = dn_-dn_+do'_-$, $dn_\pm = d\epsilon_\pm do_\pm \epsilon^2_\pm \beta_\pm f_\pm$, and the Jacobian is

$$J_{\rm bs} = \frac{\epsilon'_+\beta'_+}{(\epsilon'_- + \epsilon'_+)\beta'_- - (\epsilon_-\beta_-\mathbf{b}_- + \epsilon_+\beta_+\mathbf{b}_+)\cdot\mathbf{b}'_-}. \quad \text{(C41)}$$

Analogously to the case of pair creation and annihilation in Sec. C 2, the energies of final-state particles are given by (C18) with the coefficients $\breve{A} = (\epsilon_- + \epsilon_+)^2 - (\epsilon_-\beta_-\mathbf{b}_- \cdot \mathbf{b}'_- + \epsilon_+\beta_+\mathbf{b}_+\cdot\mathbf{b}'_-)^2$, $\breve{B} = (\epsilon_- + \epsilon_+)[m^2c^4 + \epsilon_-\epsilon_+(1 - \beta_-\beta_+\mathbf{b}_-\cdot\mathbf{b}_+)]$, $\breve{C} = [m^2c^4 + \epsilon_-\epsilon_+(1 - \beta_-\beta_+\mathbf{b}_-\cdot\mathbf{b}_+)]^2 + m^2c^4[\epsilon_-\beta_-\mathbf{b}_-\cdot\mathbf{b}'_- + \epsilon_+\beta_+\mathbf{b}_+\cdot\mathbf{b}'_-]^2$. In order to select the correct root, one has to check the condition (C33), changing the subscripts $1 \to -$, $2 \to +$.

APPENDIX D: BINARY REACTIONS WITH PROTONS

1. Compton scattering on protons, $\gamma p \to \gamma' p'$

The rate for this process $t^{-1}_{\gamma p}$ compared to the rate of Compton scattering of electrons $t^{-1}_{\gamma e}$ is much longer,

$$t^{-1}_{\gamma p} = \frac{n_p}{n_\pm}\left(\frac{\epsilon_\pm}{Mc^2}\right)^2 t^{-1}_{\gamma e}, \qquad \epsilon \geq mc^2. \quad \text{(D1)}$$

Moreover, it is longer than any time scale for binary and triple reactions considered in this paper, and thus we exclude this reaction from the computations.

2. Electron-proton and positron-proton scattering, $e_\pm p \to e'_\pm p'$

The time evolution of the distribution functions of electrons due to $ep \to e'p'$ is described by

$$\left(\frac{\partial f_\pm(\mathbf{p},t)}{\partial t}\right)_{ep\to e'p'} = \int d\mathbf{q}d\mathbf{p}'d\mathbf{q}' V w_{\mathbf{p}',\mathbf{q}';\mathbf{p},\mathbf{q}}[f_\pm(\mathbf{p}',t) \times f_p(\mathbf{q}',t) - f_\pm(\mathbf{p},t) f_p(\mathbf{q},t)], \quad \text{(D2)}$$

$$\left(\frac{\partial f_p(\mathbf{q},t)}{\partial t}\right)_{ep\to e'p'} = \int d\mathbf{p}d\mathbf{p}'d\mathbf{q}' V w_{\mathbf{p}',\mathbf{q}';\mathbf{p},\mathbf{q}}[f_\pm(\mathbf{p}',t) \times f_p(\mathbf{q}',t) - f_\pm(\mathbf{p},t) f_p(\mathbf{q},t)], \quad \text{(D3)}$$

where

$$w_{\mathbf{p}',\mathbf{q}';\mathbf{p},\mathbf{q}} = \frac{\hbar^2c^6}{(2\pi)^2 V}\delta(\epsilon_e + \epsilon_p - \epsilon'_e - \epsilon'_p) \times \delta(\mathbf{p} + \mathbf{q} - \mathbf{p}' - \mathbf{q}')\frac{|M_{fi}|^2}{16\epsilon_e\epsilon_p\epsilon'_e\epsilon'_p}, \quad \text{(D4)}$$

$$|M_{fi}|^2 = 2^6\pi^2\alpha^2\frac{1}{t^2}\left\{\frac{1}{2}(s^2 + u^2) + (m^2c^2 + M^2c^2) \times (2t - m^2c^2 - M^2c^2)\right\}. \quad \text{(D5)}$$

The invariants are $s = (\mathfrak{p} + \mathfrak{q})^2 = m^2c^2 + M^2c^2 + 2\mathfrak{p}\cdot\mathfrak{q}$, $t = (\mathfrak{p} - \mathfrak{p}')^2 = 2(m^2c^2 - \mathfrak{p}\cdot\mathfrak{p}') = 2(M^2c^2 - \mathfrak{q}\cdot\mathfrak{q}')$ and $u = (\mathfrak{p} - \mathfrak{q}')^2 = m^2c^2 + M^2c^2 - 2\mathfrak{p}\cdot\mathfrak{q}'$, $s + t + u = 2(m^2c^2 + M^2c^2)$. The energies of the particles after the interaction are given by (C18) with $\bar{A} = (\epsilon_\pm + \epsilon_p)^2 - [(\epsilon_\pm\beta_\pm\mathbf{b}_\pm + \epsilon_p\beta_p\mathbf{b}_p)\cdot\mathbf{b}'_\pm]^2$, $\bar{B} = (\epsilon_\pm + \epsilon_p)\times[m^2c^4 + \epsilon_\pm\epsilon_p(1 - \beta_\pm\beta_p\mathbf{b}_\pm\cdot\mathbf{b}_p)]$, $\bar{C} = m^2c^4\{(\epsilon_\pm\beta_\pm\mathbf{b}_\pm\cdot\mathbf{b}'_\pm + \epsilon_p\beta_p\mathbf{b}_p\cdot\mathbf{b}'_\pm)^2 + [m^2c^4 + \epsilon_\pm\epsilon_p(1 - \beta_\pm\beta_p\mathbf{b}_\pm\cdot\mathbf{b}_p)]\}^2$. The correct root is selected by the condition (C33) with the substitutions $1 \to \pm$, $2 \to p$.

Absorption and emission coefficients for this reaction are

$$(\chi E)^{ep}_{\pm,\omega} = \frac{1}{\Delta\epsilon_{\pm,\omega}} \int_{\epsilon_\pm \in \Delta\epsilon_{\pm,\omega}} dn_\pm dn_p do'_\pm J_{\rm ep} \times \frac{\epsilon'^2_\pm \beta'_\pm \epsilon_\pm |M_{fi}|^2 \hbar^2 c^2}{16\epsilon_\pm \epsilon_p \epsilon'_\pm \epsilon'_p}, \tag{D6}$$

$$(\chi E)^{ep}_{p,\omega} = \frac{1}{\Delta\epsilon_{p,\omega}} \int_{\epsilon_p \in \Delta\epsilon_{p,\omega}} dn_\pm dn_p do'_\pm J_{\rm ep} \times \frac{\epsilon'^2_\pm \beta'_\pm \epsilon_p |M_{fi}|^2 \hbar^2 c^2}{16\epsilon_\pm \epsilon_p \epsilon'_\pm \epsilon'_p}, \tag{D7}$$

$$\eta^{ep}_{\pm,\omega} = \frac{1}{\Delta\epsilon_{\pm,\omega}} \int_{\epsilon'_\pm \in \Delta\epsilon_{\pm,\omega}} dn_\pm dn_p do'_\pm J_{\rm ep} \times \frac{\epsilon'^2_\pm \beta'_\pm \epsilon'_\pm |M_{fi}|^2 \hbar^2 c^2}{16\epsilon_\pm \epsilon_p \epsilon'_\pm \epsilon'_p}, \tag{D8}$$

$$\eta^{ep}_{p,\omega} = \frac{1}{\Delta\epsilon_{p,\omega}} \int_{\epsilon'_p \in \Delta\epsilon_{p,\omega}} dn_\pm dn_p do'_\pm J_{\rm ep} \times \frac{\epsilon'^2_\pm \beta'_\pm \epsilon'_p |M_{fi}|^2 \hbar^2 c^2}{16\epsilon_\pm \epsilon_p \epsilon'_\pm \epsilon'_p}, \tag{D9}$$

where $dn_i = d\epsilon_i do_i \epsilon_i^2 \beta_i f_i$, $i = \pm$, p, and the Jacobian is

$$J_{\rm ep} = \frac{\epsilon'_p \beta'_p}{(\epsilon'_\pm + \epsilon'_p)\beta'_\pm - (\epsilon_p \beta_p \mathbf{b}_p + \epsilon_\pm \beta_\pm \mathbf{b}_\pm)\cdot \mathbf{b}'_\pm}. \tag{D10}$$

The rate for proton-electron (proton-positron) scattering is

$$t^{-1}_{ep} \approx \frac{\epsilon}{Mc^2} t^{-1}_{ee}, \qquad \epsilon_\pm \ll \epsilon_p. \tag{D11}$$

3. Proton-proton scattering, $p_1 p_2 \to p'_1 p'_2$

This reaction is similar to $e_1 e_2 \to e'_1 e'_2$, described in Sec. C 3. The time evolution of the distribution functions of electrons is described by

$$\left(\frac{\partial f_i(\mathbf{p}_i, t)}{\partial t}\right)_{p_1 p_2 \to p'_1 p'_2} = \int d\mathbf{q}_j d\mathbf{q}'_1 d\mathbf{q}'_2 V w_{\mathbf{q}'_1,\mathbf{q}'_2;\mathbf{q}_1,\mathbf{q}_2} [f_1(\mathbf{q}'_1, t) \times f_2(\mathbf{q}'_2, t) - f_1(\mathbf{q}_1, t) f_2(\mathbf{q}_2, t)], \tag{D12}$$

with $j = 3 - i$, and where

$$w_{\mathbf{q}'_1,\mathbf{q}'_2;\mathbf{q}_1,\mathbf{q}_2} = \frac{\hbar^2 c^6}{(2\pi)^2 V} \delta(\epsilon_1 + \epsilon_2 - \epsilon'_1 - \epsilon'_2) \times \delta(\mathbf{q}_1 + \mathbf{q}_2 - \mathbf{q}'_1 - \mathbf{q}'_2) \frac{|M_{fi}|^2}{16\epsilon_1 \epsilon_2 \epsilon'_1 \epsilon'_2}, \tag{D13}$$

$$|M_{fi}|^2 = 2^6 \pi^2 \alpha^2 \left\{ \frac{1}{t^2}\left[\frac{s^2 + u^2}{2} + 4M^2c^2(t - M^2c^2)\right] + \frac{1}{u^2}\left[\frac{s^2 + t^2}{2} + 4M^2c^2(u - M^2c^2)\right] + \frac{4}{tu}\left(\frac{s}{2} - M^2c^2\right)\left(\frac{s}{2} - 3M^2c^2\right)\right\}, \tag{D14}$$

and the invariants are $s = (\mathfrak{q}_1 + \mathfrak{q}_2)^2 = 2(M^2c^2 + \mathfrak{q}_1 \cdot \mathfrak{q}_2)$, $t = (\mathfrak{q}_1 - \mathfrak{q}'_1)^2 = 2(M^2c^2 - \mathfrak{q}_1 \cdot \mathfrak{q}'_1)$, and $u = (\mathfrak{q}_1 - \mathfrak{q}'_2)^2 = 2(M^2c^2 - \mathfrak{q}_1 \mathfrak{q}'_2)$.

For the rate we have

$$t^{-1}_{pp} \approx \sqrt{\frac{m}{M}} \frac{n_p}{n_\pm} t^{-1}_{ee}, \qquad v_p \approx \sqrt{\frac{m}{M}} v_\pm, \qquad v_\pm \approx c. \tag{D15}$$

APPENDIX E: THREE-BODY PROCESSES

We adopt emission coefficients for triple interactions from [30].

The bremsstrahlung is

$$\eta_\gamma^{e^\mp e^\mp \to e^\mp e^\mp \gamma} = (n_+^2 + n_-^2)\frac{16}{3}\frac{\alpha c}{\varepsilon}\left(\frac{e^2}{mc^2}\right)^2 \ln\left[4\xi(11.2 + 10.4\theta^2)\frac{\theta}{\varepsilon}\right]\frac{\frac{3}{5}\sqrt{2}\theta + 2\theta^2}{\exp(1/\theta)K_2(1/\theta)}, \tag{E1}$$

$$\eta_\gamma^{e^- e^+ \to e^- e^+ \gamma} = n_+ n_- \frac{16}{3}\frac{2\alpha c}{\varepsilon}\left(\frac{e^2}{mc^2}\right)^2 \ln\left[4\xi(1 + 10.4\theta^2)\frac{\theta}{\varepsilon}\right] \times \frac{\sqrt{2} + 2\theta + 2\theta^2}{\exp(1/\theta)K_2(1/\theta)}, \tag{E2}$$

$$\eta_\gamma^{pe^\pm \to p' e^{\pm\prime} \gamma} = (n_+ + n_-)n_p \frac{16}{3}\frac{\alpha c}{\varepsilon}\left(\frac{e^2}{mc^2}\right)^2 \times \ln\left[4\xi(1 + 3.42\theta)\frac{\theta}{\varepsilon}\right]\frac{1 + 2\theta + 2\theta^2}{\exp(1/\theta)K_2(1/\theta)}, \tag{E3}$$

where $\xi = e^{-0.5772}$, and $K_2(1/\theta)$ is the modified Bessel function of the second kind of order 2.

The double Compton scattering is

$$\eta_\gamma^{e^\pm \gamma \to e^{\pm\prime} \gamma' \gamma''} = (n_+ + n_-)n_\gamma \frac{128}{3}\frac{\alpha c}{\varepsilon}\left(\frac{e^2}{mc^2}\right)^2 \times \frac{\theta^2}{1 + 13.91\theta + 11.05\theta^2 + 19.92\theta^3}. \tag{E4}$$

The three-photon annihilation is

$$\eta_\gamma^{e^\pm e^\mp\to\gamma\gamma'\gamma''} = n_+ n_- \alpha c\left(\frac{e^2}{mc^2}\right)^2 \frac{1}{\varepsilon} \times \frac{\frac{4}{\theta}(2\ln^2 2\xi\theta + \frac{\pi^2}{6} - \frac{1}{2})}{4\theta + \frac{1}{\theta^2}(2\ln^2 2\xi\theta + \frac{\pi^2}{6} - \frac{1}{2})}, \quad \text{(E5)}$$

where we have joined two limiting approximations given by [30].

The radiative pair production is

$$\eta_e^{\gamma\gamma'\to\gamma''e^\pm e^\mp} = \eta_\gamma^{e^\pm e^\mp\to\gamma\gamma'\gamma''} \frac{n_\gamma^2}{n_+ n_-}\left[\frac{K_2(1/\theta)}{2\theta^2}\right]^2. \quad \text{(E6)}$$

The electron-photon pair production is

$$\eta_\gamma^{e_1^\pm\gamma\to e_1^{\pm\prime}e^\pm e^\mp} = \begin{cases}(n_+ + n_-)n_\gamma\alpha c(\frac{e^2}{mc^2})^2\exp(-\frac{2}{\theta})16.1\theta^{0.541} & \theta \le 2\\ (n_+ + n_-)n_\gamma\alpha c(\frac{e^2}{mc^2})^2(\frac{56}{9}\ln 2\xi\theta - \frac{8}{27})\frac{1}{1+0.5/\theta} & \theta > 2.\end{cases} \quad \text{(E7)}$$

The proton-photon pair production is

$$\eta_\gamma^{p\gamma\to p'e^\pm e^\mp} = \begin{cases} n_p n_\gamma\alpha c(\frac{e^2}{mc^2})^2\exp(-\frac{2}{\theta})\frac{1}{1+0.9\theta} & \theta \le 1.252\,77\\ n_p n_\gamma\alpha c(\frac{e^2}{mc^2})^2[\frac{28}{9}(\ln 2\xi\theta + 1.7) - \frac{92}{27}] & \theta > 1.252\,77.\end{cases} \quad \text{(E8)}$$

We use the absorption coefficient for three-body processes written as

$$\chi_\gamma^{3p} = \eta_\gamma^{3p}/E_\gamma^{eq}, \quad \text{(E9)}$$

where η_γ^{3p} is the sum of the emission coefficients of photons in the three-particle processes, $E_\gamma^{eq} = 2\pi\epsilon^3 f_\gamma^{eq}/c^3$, where f_γ^{eq} is given by (15).

From Eq. (22), the law of energy conservation in the three-body processes is

$$\int\sum_i(\eta_i^{3p} - \chi_i^{3p}E_i)d\mu d\epsilon = 0. \quad \text{(E10)}$$

For exact conservation of energy in these processes we introduce the following coefficients of emission and absorption for electrons:

$$\chi_e^{3p} = \frac{\int(\eta_\gamma^{3p} - \chi_\gamma^{3p}E_\gamma)d\epsilon d\mu}{\int E_e d\epsilon d\mu}, \qquad \eta_e^{3p} = 0, \qquad \int(\eta_\gamma^{3p} - \chi_\gamma^{3p}E_\gamma)d\epsilon d\mu > 0, \quad \text{(E11)}$$

or

$$\frac{\eta_e^{3p}}{E_e} = -\frac{\int(\eta_\gamma^{3p} - \chi_\gamma^{3p}E_\gamma)d\epsilon d\mu}{\int E_e d\epsilon d\mu}, \qquad \chi_e^{3p} = 0, \qquad \int(\eta_\gamma^{3p} - \chi_\gamma^{3p}E_\gamma)d\epsilon d\mu < 0. \quad \text{(E12)}$$

APPENDIX F: CUTOFF IN COULOMB SCATTERING

Denote quantities in the center-of-mass (CM) frame with the index 0 and with a prime after the interaction. Suppose we have two particles with masses m_1 and m_2. The change of the angle of the first particle in the CM system is

$$\theta_{10} = \arccos(\mathbf{b}_{10}\cdot\mathbf{b}'_{10}), \quad \text{(F1)}$$

the numerical grid size is $\Delta\theta_g$, and the minimal angle at the scattering is $\theta_{\min}$.

By definition, in the CM frame

$$\mathbf{p}_{10} + \mathbf{p}_{20} = 0, \quad \text{(F2)}$$

where

$$\mathbf{p}_{i0} = \mathbf{p}_i + \left[(\Gamma - 1)(\mathbf{N}\mathbf{p}_i) - \Gamma\frac{V}{c}\frac{\epsilon_i}{c}\right]\mathbf{N}, \qquad i = 1, 2, \quad \text{(F3)}$$

and

$$\epsilon_i = \Gamma(\epsilon_{i0} + \mathbf{V}\mathbf{p}_{i0}). \quad \text{(F4)}$$

Then for the velocity of the CM frame we have

$$\frac{\mathbf{V}}{c} = c\frac{\mathbf{p}_1 + \mathbf{p}_2}{\epsilon_1 + \epsilon_2}, \qquad \mathbf{N} = \frac{\mathbf{V}}{V}, \qquad \Gamma = \frac{1}{\sqrt{1 - (\frac{V}{c})^2}}. \quad \text{(F5)}$$

By definition,

$$\mathbf{b}_{10} = \mathbf{b}_{20}, \quad \mathbf{b}'_{10} = \mathbf{b}'_{20}, \quad \text{(F6)}$$

and then

$$|\mathbf{p}_{10}| = |\mathbf{p}_{20}| = p_0 \equiv \frac{1}{c}\sqrt{\epsilon_{10}^2 - m_1^2c^4} = \frac{1}{c}\sqrt{\epsilon_{20}^2 - m_2^2c^4}, \quad \text{(F7)}$$

where

$$\epsilon_{10} = \frac{(\epsilon_1 + \epsilon_2)^2 - \Gamma^2(m_2^2 - m_1^2)c^4}{2(\epsilon_1 + \epsilon_2)\Gamma}, \quad \text{(F8)}$$

$$\epsilon_{20} = \frac{(\epsilon_1 + \epsilon_2)^2 + \Gamma^2(m_2^2 - m_1^2)c^4}{2(\epsilon_1 + \epsilon_2)\Gamma}. \quad \text{(F9)}$$

Haug [44] gives the minimal scattering angle in the center-of-mass system as follows:

$$\theta_{\min} = \frac{2\hbar}{\mathcal{M}cD} \frac{\gamma_r}{(\gamma_r + 1)\sqrt{2(\gamma_r - 1)}}, \tag{F10}$$

where $\mathcal{M}$, as above, is the reduced mass, the maximum impact parameter (neglecting the effect of protons) is

$$D = \frac{c^2}{\omega} \frac{p_0}{\epsilon_{10}}, \tag{F11}$$

and the invariant Lorentz factor of relative motion (e.g. [44]) is

$$\gamma_r = \frac{1}{\sqrt{1 - (\frac{v_r}{c})^2}} = \frac{\epsilon_1\epsilon_2 - \mathbf{p}_1\mathbf{p}_2c^2}{m_1m_2c^4}. \tag{F12}$$

In the CM frame we finally obtain

$$t_{\min} = 2\left[(mc)^2 - \left(\frac{\epsilon_{10}}{c}\right)^2(1 - \beta_{10}^2\cos\theta_{\min})\right].$$

Since it is invariant, we then replace t in the denominator of $|M_{fi}|^2$ in (C32) by the value $t\sqrt{1 + t_{\min}^2/t^2}$ to implement the cutoff scheme. Considering the scattering of identical particles we remove the case of exchange of particles as well as scattering on small angles; in other words, we change u in the denominator of $|M_{fi}|^2$ in (C32), (D5), and (D14) by the value $u\sqrt{1 + t_{\min}^2/u^2}$.

APPENDIX G: MASS SCALING FOR THE PROTON-ELECTRON/POSITRON REACTION

Since the proton mass is larger than electron mass-energy $M \gg m, \epsilon$, then for the CM frame

$$\mathbf{V} \approx \frac{\mathbf{p}_1 + \mathbf{p}_2}{M}, \qquad \Gamma \approx 1, \qquad J_1 \approx 1, \tag{G1}$$

$$\epsilon_1' - \epsilon_1 \approx \mathbf{V}(\mathbf{e}_{01}' - \mathbf{e}_{01})p_0 \propto \frac{1}{M}, \tag{G2}$$

and also

$$\frac{s^2}{c^4} \approx M^4 + 4mM^3 + 6m^2M^2, \tag{G3}$$

$$\frac{u^2}{c^4} \approx M^4 - 4mM^3 + 6m^2M^2, \tag{G4}$$

$$|M_{fi}|^2 \propto \frac{1}{t^2}(6m^2 - 2t)M^2, \tag{G5}$$

while

$$t = \frac{-2m^2\beta_{e0}^2(1 - \mathbf{e}_{e0}\mathbf{e}_{e0}')}{1 - \beta_{e0}^2} = \frac{-2m^2\beta_e^2(1 - \mathbf{e}_e\mathbf{e}_e')}{1 - \beta_e^2}[1 + O(M^{-1})] \tag{G6}$$

for small angles.

This leads to the following scaling for the reaction rate:

$$\eta_{e\omega}^{ep} - (\chi E)_{e\omega}^{ep} \propto \int \frac{(\epsilon_e' - \epsilon_e)|M_{fi}|^2}{\epsilon_e\epsilon_p\epsilon_e'\epsilon_p'} \propto \frac{1}{M}. \tag{G7}$$

We can therefore calculate $\eta_{e\omega}^{ep_0}$, $(\chi E)_{e\omega}^{ep_0}$ for a pseudoparticle with mass $M_0 \gg m$, ϵ instead of M and obtain

$$\eta_{e\omega}^{ep} \approx \frac{M_0}{M}\eta_{e\omega}^{ep_0}, \tag{G8}$$

$$(\chi E)_{e\omega}^{ep} \approx \frac{M_0}{M}(\chi E)_{e\omega}^{ep_0}. \tag{G9}$$

For such purposes we selected the mass of this pseudoparticle as $M_0 = 20m$.

APPENDIX H: THE DEFINITION OF MATRIX ELEMENTS

Following [41] we define the scattering matrix, which is composed of real and imaginary parts,

$$S_{fi} = \delta_{fi} + i(2\pi\hbar)^4\delta^{(4)}(\mathfrak{p}_f - \mathfrak{p}_i)T_{fi}, \tag{H1}$$

where δ_{fi} is the unity matrix, $\delta^{(4)}$ stands for the four-momentum conservation, and the elements of T_{fi} are scattering amplitudes.

The transition probability of a given process per unit time is then

$$w_{fi} = c(2\pi\hbar)^4\delta^{(4)}(\mathfrak{p}_f - \mathfrak{p}_i)|T_{fi}|^2V, \tag{H2}$$

where V is the normalization volume.

For a process involving a outgoing particles and b incoming particles, the differential probability per unit time is defined as

$$dw = c(2\pi\hbar)^4\delta^{(4)}(\mathfrak{p}_f - \mathfrak{p}_i)|M_{fi}|^2V \times \left[\prod_b \frac{\hbar c}{2\epsilon_bV}\right] \times \left[\prod_a \frac{d\mathbf{p}_a'}{(2\pi\hbar)^3}\frac{\hbar c}{2\epsilon_a'}\right], \tag{H3}$$

where $\mathbf{p}_a'$ and ϵ_a' are, respectively, momenta and energies of outgoing particles, ϵ_b are energies of particles before the interaction, M_{fi} are the corresponding matrix elements, $\delta^{(4)}$ stands for energy-momentum conservation, and V is the normalization volume. The matrix elements are related to the scattering amplitudes by

$$M_{fi} = \left[\prod_b \frac{\hbar c}{2\epsilon_bV}\right]\left[\prod_a \frac{\hbar c}{2\epsilon_a'V}\right]T_{fi}. \tag{H4}$$

For a binary process with two incoming and two outgoing particles, it is convenient to introduce the differential cross section. In fact, the differential probability for incoming particles with four-momenta $\mathfrak{p}_1$ and $\mathfrak{p}_2$, energies ϵ_1 and ϵ_2, and masses m_1 and m_2, respectively, is just the product of the differential cross section and the flux den-

sity,

$$dw = j d\sigma, \tag{H5}$$

where

$$j = \frac{cI}{\epsilon_1 \epsilon_2 V}, \tag{H6}$$

$$I = c\sqrt{\mathfrak{p}_1\mathfrak{p}_2 - m_1 m_2 c^2}. \tag{H7}$$

In the CM reference frame the relation between the cross section and $|M_{fi}|^2$ acquires the simplest form if the cross section does not depend on the azimuth of $\mathbf{p}_1'$ relative to $\mathbf{p}_1$; then,

$$d\sigma = \frac{\hbar^2 c^4}{64\pi} |M_{fi}|^2 \frac{dt}{I}, \tag{H8}$$

$$t = (\mathfrak{p}_1 - \mathfrak{p}_2)^2, \tag{H9}$$

$$dt = 2|\mathbf{p}_1||\mathbf{p}_1'| d\cos\vartheta, \tag{H10}$$

where ϑ is the angle between $\mathbf{p}_1$ and $\mathbf{p}_1'$.

[1] S. Weinberg, *Gravitation and Cosmology: Principles and Applications of the General Theory of Relativity* (Wiley-VCH, New York, 1972), p. 688, ISBN 0-471-92567-5.
[2] E. W. Kolb and M. S. Turner, *The Early Universe*, Frontiers in Physics (Addison-Wesley, Reading, MA, 1990).
[3] W. T. Hu, Ph.D. thesis, University of California, Berkeley, 1995.
[4] S. Weinberg, *Cosmology* (Oxford University Press, New York, 2008).
[5] J. Goodman, Astrophys. J. **308**, L47 (1986).
[6] T. Piran, Phys. Rep. **314**, 575 (1999).
[7] R. Ruffini, J. D. Salmonson, J. R. Wilson, and S.-S. Xue, Astron. Astrophys. **350**, 334 (1999).
[8] J. F. C. Wardle, D. C. Homan, R. Ojha, and D. H. Roberts, Nature (London) **395**, 457 (1998).
[9] E. Churazov, R. Sunyaev, S. Sazonov, M. Revnivtsev, and D. Varshalovich, Mon. Not. R. Astron. Soc. **357**, 1377 (2005).
[10] V. V. Usov, Phys. Rev. Lett. **80**, 230 (1998).
[11] D. B. Blaschke, A. V. Prozorkevich, C. D. Roberts, S. M. Schmidt, and S. A. Smolyansky, Phys. Rev. Lett. **96**, 140402 (2006).
[12] I. Kuznetsova, D. Habs, and J. Rafelski, Phys. Rev. D **78**, 014027 (2008).
[13] G. S. Bisnovatyi-Kogan, Y. B. Zel'Dovich, and R. A. Syunyaev, Sov. Astron. **15**, 17 (1971).
[14] T. A. Weaver, Phys. Rev. A **13**, 1563 (1976).
[15] A. P. Lightman, Astrophys. J. **253**, 842 (1982).
[16] R. J. Gould, Astrophys. J. **254**, 755 (1982).
[17] S. Stepney and P. W. Guilbert, Mon. Not. R. Astron. Soc. **204**, 1269 (1983).
[18] P. S. Coppi and R. D. Blandford, Mon. Not. R. Astron. Soc. **245**, 453 (1990).
[19] A. P. Lightman and D. L. Band, Astrophys. J. **251**, 713 (1981).
[20] R. Svensson, Astrophys. J. **258**, 335 (1982).
[21] P. W. Guilbert and S. Stepney, Mon. Not. R. Astron. Soc. **212**, 523 (1985).
[22] A. A. Zdziarski, Astrophys. J. **283**, 842 (1984).
[23] R. J. Gould, Phys. Fluids **24**, 102 (1981).
[24] S. Stepney, Mon. Not. R. Astron. Soc. **202**, 467 (1983).
[25] R. Svensson, Astrophys. J. **258**, 321 (1982).
[26] R. J. Gould, Astrophys. J. **238**, 1026 (1980).
[27] E. Haug, Astron. Astrophys. **148**, 386 (1985).
[28] A. P. Lightman, Astrophys. J. **244**, 392 (1981).
[29] R. J. Gould, Astrophys. J. **285**, 275 (1984).
[30] R. Svensson, Mon. Not. R. Astron. Soc. **209**, 175 (1984).
[31] S. Iwamoto and F. Takahara, Astrophys. J. **601**, 78 (2004).
[32] G. Cavallo and M. J. Rees, Mon. Not. R. Astron. Soc. **183**, 359 (1978).
[33] L. D. Landau and E. M. Lifshitz, *Physical Kinetics* (Elsevier, Oxford, 1981).
[34] A. G. Aksenov, R. Ruffini, and G. V. Vereshchagin, Phys. Rev. Lett. **99**, 125003 (2007).
[35] A. G. Aksenov, R. Ruffini, and G. V. Vereshchagin, *Thermalization of Electron-Positron-Photon Plasmas with an Application to GRB* (AIP, New York, 2008), Vol. 966, pp. 191–196.
[36] R. Ruffini *et al.*, *The Blackholic Energy and the Canonical Gamma-Ray Burst* (AIP, New York, 2007), Vol. 910, pp. 55–217.
[37] S. Belyaev and G. Budker, Dokl. Akad. Nauk SSSR **107**, 807 (1956) Sov. Phys. Dokl. **1**, 218 (1956)].
[38] D. Mihalas and B. W. Mihalas, *Foundations of Radiation Hydrodynamics* (Oxford University Press, New York, 1984).
[39] A. G. Aksenov, M. Milgrom, and V. V. Usov, Astrophys. J. **609**, 363 (2004).
[40] D. Lemoine, Phys. Rev. D **51**, 2677 (1995).
[41] V. B. Berestetskii, E. M. Lifshitz, and V. B. Pitaevskii, *Quantum Electrodynamics* (Elsevier, Oxford, 1982).
[42] W. Greiner and J. Reinhardt, *Quantum Electrodynamics* (Springer, Berlin, 2003).
[43] A. Akhiezer and V. Berestetskii, *Quantum Electrodynamics* (Nauka, Moscow, 1981).
[44] E. Haug, Astron. Astrophys. **191**, 181 (1988).
[45] R. P. Pilla and J. Shaham, Astrophys. J. **486**, 903 (1997).
[46] J. Ehlers, in *Survey of General Relativity Theory*, edited by W. Israel, Relativity, Astrophysics and Cosmology (Reidel, Dordrecht, 1973), pp. 1–125.
[47] G. Hall and J. M. Watt, *Modern Numerical Methods for Ordinary Differential Equations* (Oxford University Press, New York, 1976).

[48] R. Ruffini, J. D. Salmonson, J. R. Wilson, and S.-S. Xue, Astron. Astrophys. **359**, 855 (2000).
[49] R. Ruffini, G. Vereshchagin, and S.-S. Xue, Phys. Rep. (to be published).
[50] M. H. Thoma, arXiv:0801.0956.
[51] N. Chernikov, Acta Phys. Pol. **23**, 629 (1963).
[52] I. P. Ochelkov, O. F. Prilutskii, I. L. Rozental, and V. V. Usov, *Relativistic Kinetics and Hydrodynamics* (Atomizdat, Moscow, 1979).